

International Atomic Energy Agency

INDC(CCP)-292/L

INDC

INTERNATIONAL NUCLEAR DATA COMMITTEE

TRANSLATION OF SELECTED PAPERS PUBLISHED

IN NUCLEAR CONSTANTS 2, 1985

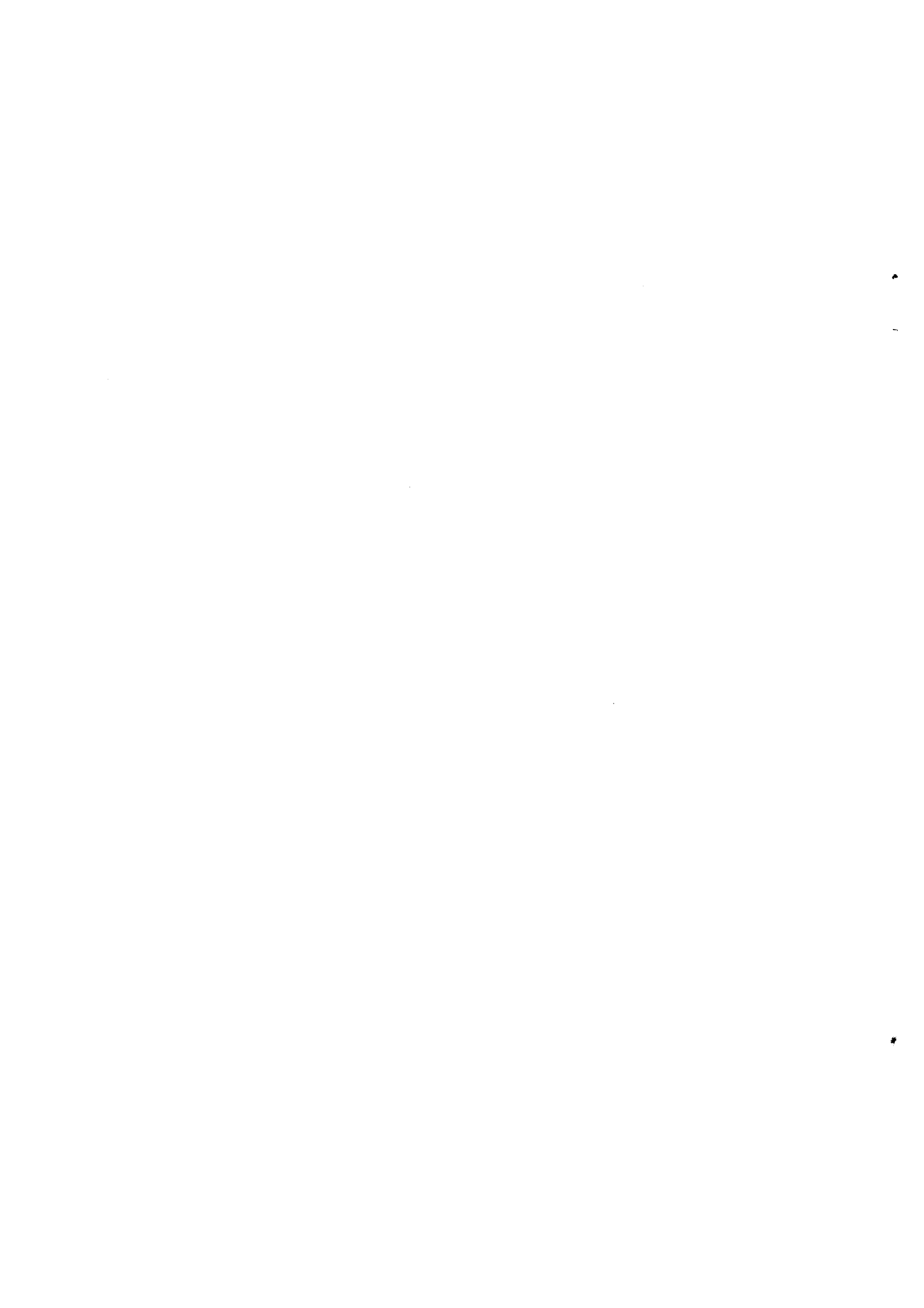
(Original Report in Russian was distributed
as INDC(CCP)-248/G)



Translated by the IAEA

January 1989

IAEA NUCLEAR DATA SECTION, WAGRAMERSTRASSE 5, A-1400 VIENNA



TRANSLATION OF SELECTED PAPERS PUBLISHED
IN NUCLEAR CONSTANTS 2, 1985
(Original Report in Russian was distributed
as INDC(CCP)-248/G)

Translated by the IAEA

January 1989

Reproduced by the IAEA in Austria
January 1989

89-00153

Contents

Incorporation of Internal Conversion Coefficients into the ENSDF Data Sets A.E. Ignatochkin, T.D. Potanina, E.N. Shurshikov	5
The Angular Anisotropy of Fragments of ^{235}U Fission Induced by 0.014-7.15 MeV Neutrons Kh.D. Androsenko, G.G. Korolev, D.L. Shpak	11
The Average Kinetic Energy of Fission Fragments V.G. Vorob'eva, B.D. Kuz'minov	15
The Dependence of the Fission Cross-Sections for Heavy Nuclei on Neutron Energy in the "Plateau" Region G.N. Smirenkin, B.I. Fursov	19
Evaluation of the Energy Dependence of the Average Number of Prompt Neutrons $\bar{\nu}_p$ for Neutron-Induced Fission of ^{235}U in the 0-20 MeV Energy Range V.V. Malinovskij, M.S. Tarasko	27
The Experimental Determination of Resonance Self- Shielding Factors Affecting the Neutron Radiative Capture Cross-Section for ^{238}U in the 10 to 140 keV Energy Range V.N. Kononov, E.D. Poletaev, M.V. Bokhovko, L.E. Kazakov, V.M. Timokhov, A.A. Voevodskiy	31
Measurement of the Neutron Radiative Capture Cross- Sections for ^{236}U and ^{197}Au in the 3-420 keV Energy Range L.E. Kazakov, V.N. Kononov, E.D. Poletaev, M.V. Bokhovko, A.A. Voevodskij, V.M. Timokhov	35

INCORPORATION OF INTERNAL CONVERSION COEFFICIENTS
INTO THE ENSDF DATA SETS

A.E. Ignatochkin, T.D. Potanina, E.N. Shurshikov

A program for automatic incorporation of internal conversion coefficients into the ENSDF data sets was developed. The program is based on modern computer calculations of these quantities.

The wide use of the achievements of nuclear physics for applied purposes has been accompanied by a growing demand for evaluated nuclear data on the structure of specific nuclei. The laborious nature of the evaluation and the need for periodic repetition of the work to take account of new experimental results have required international co-operation, which is now being implemented within the framework of an International network of co-operating centres [1]. A unified format for presentation of evaluated data was required, with, where possible, unified evaluation procedures to facilitate comparison of evaluations. Computing techniques and machine-readable media facilitate the use and exchange of data.

The ENSDF format [2] has been adopted for the presentation of data on nuclear structure, making it possible to record the many characteristics of nuclear states and transitions between them. One of these characteristics is the internal conversion coefficient (ICC), which is significant in the evaluation and interpretation of other decay characteristics. For the evaluated ICC, a theoretical value is taken, obtained from model calculations. In practice, ICC evaluation can be divided into two stages: the first is the selection of a model, and the construction of ICC tables based on it for given nuclear charges and various transition energy values; the second is the interpolation of tabular values to a specific transition energy.

Papers have been published showing the results of calculating ICC tables for the K, L and M shells [3-5], as well as papers [6] assessing the influence of the contribution of higher shells to the full ICC. Some aspects of these papers are still being discussed [7], but in preparing data for the ENSDF format the set of data in Refs [3, 6] is usually used, together with the results in Ref. [4] for nuclei with charges not included in the calculation in Ref. [3]. Such tables are prepared on a machine-readable medium and distributed within the International network of co-operating centres. The NSICC program [8] is distributed with them to facilitate interpolation of the tables, as it provides for reception of the required parameters directly from the processed data set in the ENSDF format and the inclusion of results in this set in accordance with the rules of the format.

Unfortunately, the NSICC program cannot be used at the Atomic and Nuclear Data Centre (TsAYaD) of the State Committee on the Utilization of Atomic Energy, as it requires a significantly greater amount of operational storage and disk memory than is available in the TsAYaD information search system, which is based on a small 1010B computer. Furthermore, the comparison of data from different tables is often required during evaluation. For the purposes of evaluations carried out at the Centre for transmission to the International network of co-operating centres, a more compact ENSICC interpolation program has been established, based on the technical resources available and making it possible to use not only the NSICC program tables, but also the tables published in Ref. [4], and when necessary other similar data on a machine-readable medium. The ENSICC retains all the features of the

NSICC program and takes into account the special features of the small 1010B computer, thus ensuring the rapid fulfilment of a given task. The choice of tables and reference to the processed data set in the ENSDF format is carried out on-line from the keyboard. In addition to the data set with the incorporated ICC, the ENSICC program permits the operator to obtain a printout of supplementary information.

Let us consider a specific example of the ENSICC program's operation. Table 1 shows the text of an evaluated data set describing a fragment from ^{166}Ho nuclear decay, in the form in which it enters the ENSICC program. According to the rules of the ENSDF format [2], the fourth and fifth positions of each line show the chemical symbol of the product nucleus. The program determines the nuclear charge from the chemical symbol taken from the first line of the set. Further analysis is made only of those lines in which the sixth to eighth positions contain the designations " $_ _ G$ ", " $I _ G$ " or " $2 _ G$ ", where the symbol " $_$ " represents a space. According to the above rules, the first two designations are equivalent to one another and serve to identify the G-lines, containing the basic data on γ -transitions. More specifically, this data includes the transition energy in kiloelectron volts (which is shown in the field from the 10th to 19th line positions) and the multipolarity of the transition or a mixture of two multipolarities (recorded in positions 32-41). If a mixture is indicated, then in field positions 42-49 there is an experimentally evaluated value of the mixing parameter, and from the 50th to 55th positions there is the uncertainty of this value (it may be asymmetric). The characteristics listed are accepted by the ENSICC program as input transition parameters, if the multipolarity field contains the data.

The incoming data are grouped in packets covering up to 100 transitions. The transition data from one packet are processed in parallel. However one data set in the ENSDF format may give rise to several packets processed in sequence, as the number of lines considered in a set is practically unlimited. The spline-interpolation method is used for calculations, as in the NSICC program. Table 2 shows the text of the same data set as in Table 1, subsequent to ENSICC processing. It will be seen that the G-lines processed

Table 1. Part of a data set in the ENSDF format, describing ^{166}Ho β -decay, prior to ENSICC program processing

166ER	166HO B-	DECAY (1200 Y)			75NDS	770505
166ER	N	0,73	5			
166HO	P	5	2(7-)	1.20E3 Y	18	1856,5 14
166ER	L	0,0	0+	STABLE		
166ER	L	80,574	82+	1,87 NS	3	
166ER	G	80,574	812.5	6E2		C
166ER	L	264,98	24+	118 PS	5	
166ER	G	184,407	1573,2	37E2		CC
166ER	L	545,44	36+			
166ER	G	280,456	2029,8	15E2		CC
166ER	L	859,38	23+			
166ER	G	594,37	30.70	4E2+M1	-8	+15-3
166ER	G	778,82	43,30	17IF E2		C
166ER	L	911,18	48+			
166ER	G	365,739	252,52	13E2		C
166ER	L	956,20	24+			
166ER	G	691,21	51,53	8E2+M1	3,3	+30-12
166ER	G	875,64	50,79	6		

Table 2. Part of a data set in the ENSDF format, after ENSICC processing

166ER	166HO B-	DECAY (1200 Y)				75NDS	840626
166ER	N	0.73	5				
166HO	P	5	2(7-)	1.20E3 Y	18	1856.5	14
166ER	L	0.0	0+	STABLE			
166ER	L	80.574	82+	1.07 NS	3		
166ER	G	80.574	812.5			6.88	C
166ER2	G	KC= 1.71	\$LC= 3.95	\$MC= 0.96		\$N+= 0.262	\$
166ER	L	264.98	24+	118 PS	5		
166ER	G	184.407	1573.2			0.334	CC
166ER2	G	KC= 0.207	\$LC= 0.097	\$MC= 0.0231		\$N+=0.00639	\$
166ER	L	545.44	36+				
166ER	G	280.456	2029.8			0.085	CC
166ER2	G	KC= 0.0615	\$LC= 0.0185	\$MC=0.00432		\$N+=0.00118	\$
166ER	L	859.38	23+				
166ER	G	594.37	30.70	4E2+M1	-8	+15-3 0.0110	
166ER2	G	KC= 0.0088	\$LC=0.00160				\$
166ER	G	778.82	43.30	17IF E2		0.00577	C
166ER2	G	KC=0.00473	\$LC= 779E-6				\$
166ER	L	911.18	48+				
166ER	G	365.739	252.52	13E2		0.0387	C
166ER2	G	KC= 0.0294	\$LC=0.00715	\$MC=0.00165		\$N+= 446E-6	\$
166ER	L	956.20	24+				
166ER	G	691.21	51.53	8E2+M1	3.3	+30-12 0.0082	8
166ER2	G	KC= 0.0067	\$LC=0.00113				8\$
166ER	G	875.64	50.79	6			

Table 3. Further data on the ICC transition shown in Table 2

ICC (WAGER) FOR Z= 68, E= 691.210 KEV.										
	E1	E2	E3	E4	E5	M1	M2	M3	M4	M5
K	2.39E-03	6.15E-03	1.43E-02	3.19E-02	ABSENT	1.33E-02	3.60E-02	8.12E-02	1.77E-01	ABSENT
L1	2.91E-04	7.77E-04	1.94E-03	4.79E-03	ABSENT	1.77E-03	5.19E-03	1.27E-02	3.05E-02	ABSENT
L2	1.82E-05	1.90E-04	1.17E-03	5.12E-03	ABSENT	1.12E-04	4.96E-04	1.75E-03	5.64E-03	ABSENT
L3	1.78E-05	8.86E-05	3.55E-04	1.27E-03	ABSENT	1.64E-05	1.07E-04	8.49E-04	4.62E-03	ABSENT
TOTAL-L	3.27E-04	1.06E-03	3.47E-03	1.12E-02	ABSENT	1.90E-03	5.79E-03	1.53E-02	4.08E-02	ABSENT
K/L	7.30E+00	5.83E+00	4.12E+00	2.85E+00	ABSENT	8.99E+00	6.22E+00	5.30E+00	4.35E+00	ABSENT
K+L,33L	2.82E-03	7.55E-03	1.89E-02	4.08E-02	ABSENT	1.58E-02	4.37E-02	1.02E-01	2.31E-01	ABSENT
M1	ENERGY OUTSIDE TABLE RANGE FOR THIS SHELL					ENERGY OUTSIDE TABLE RANGE FOR THIS SHELL				
M2	ENERGY OUTSIDE TABLE RANGE FOR THIS SHELL					ENERGY OUTSIDE TABLE RANGE FOR THIS SHELL				
M3	ENERGY OUTSIDE TABLE RANGE FOR THIS SHELL					ENERGY OUTSIDE TABLE RANGE FOR THIS SHELL				
M4	ENERGY OUTSIDE TABLE RANGE FOR THIS SHELL					ENERGY OUTSIDE TABLE RANGE FOR THIS SHELL				
M5	ENERGY OUTSIDE TABLE RANGE FOR THIS SHELL					ENERGY OUTSIDE TABLE RANGE FOR THIS SHELL				
N+0+ FROM DRAGON	ABSENT	ABSENT	ABSENT	ABSENT	ABSENT	ABSENT	ABSENT	ABSENT	ABSENT	ABSENT
FOR MULTIPOLE: E2+M1 MIX, RAT. 3.3 +30-12:										
	ICC	ICC+DICC	ICC-DICC							
K	6.75E-03	6.32E-03	7.46E-03							
L1	8.60E-04	8.01E-04	9.60E-04							
L2	1.83E-04	1.88E-04	1.75E-04							
L3	8.25E-05	8.68E-05	7.53E-05							
TOTAL-L	1.13E-03	1.08E-03	1.21E-03							
K/L	5.99E+00	5.88E+00	6.17E+00							
K+L,33L	8.24E-03	7.76E-03	9.07E-03							
M1	ABSENT	ABSENT	ABSENT							
M2	ABSENT	ABSENT	ABSENT							
M3	ABSENT	ABSENT	ABSENT							
M4	ABSENT	ABSENT	ABSENT							
M5	ABSENT	ABSENT	ABSENT							
TOTAL-M	ABSENT	ABSENT	ABSENT							
M/L	ABSENT	ABSENT	ABSENT							
K+L+M,33M	ABSENT	ABSENT	ABSENT							
N+0+ FROM DRAGON	ABSENT	ABSENT	ABSENT							
K+L+M+NO+	ABSENT	ABSENT	ABSENT							
=====										
166ER	G 691.21	51.53	8E2+M1	3.3	+30-12	0.0082	8			
166ER2	G XC= 0.0067	73LC=0.00113	8\$							
166ER	G 875.64	50.79	6							

by the program show, in field positions 56-62, the value of the conversion coefficient. If the G-line shows a mixture, then the ICC uncertainty, conditioned by the uncertainty in the multipolarity mixture parameter, may be given in positions 64 and 65. Where the uncertainty is not given, it is within the limits of the table's accuracy, estimated at 3%.

In the lines identified by the above designation "2 \square G", ICC data is given for the shells for which it is known. In these lines data units are determined by the identifiers KC, LC, MC and N+ for K-, L-, M- and higher shells respectively, followed by the coefficient values. As in the case of the full ICC, the "2 \square G" lines may indicate uncertainties. However in this case the uncertainty is separated from the value by at least one space. The ICC data for different shells are separated by a dollar sign.

If the ICC field in the G-line with known multipolarity contained data prior to processing, then the former value is lost as is the former data from the "2 \square G" line. New values are not calculated for a known transition multipolarity, but the old values, if any, are retained.

As previously mentioned, the program will print out further information at the operator's request. Table 3 is an example of such a print-out containing detailed information on the formation of the lines underlined in Table 2. Similar information is given for all processed transitions directly preceding the G-line to which it relates in the full text of the set. The lower part of Table 3 is only given if there is a multipolarity mixture for a given mixing parameter. It is seen that the conversion coefficients are calculated for each transition energy and all multipoles at all sub-shells and shells for which this is possible in the tables; the ratios of conversion coefficients at the K- and L-shells, M- and L-shells; different evaluations for the full ICC. In the case of a multipolarity mixture, the same characteristics are calculated for the mean mixing parameter and the limiting values for a given uncertainty.

This program is used for preparing data for the international ENSDF file at the Atomic and Nuclear Data Centre.

THE ANGULAR ANISOTROPY OF FRAGMENTS OF ^{235}U FISSION
INDUCED BY 0.014-7.15 MeV NEUTRONS

Kh.D. Androsenko, G.G. Korolev, D.L. Shpak

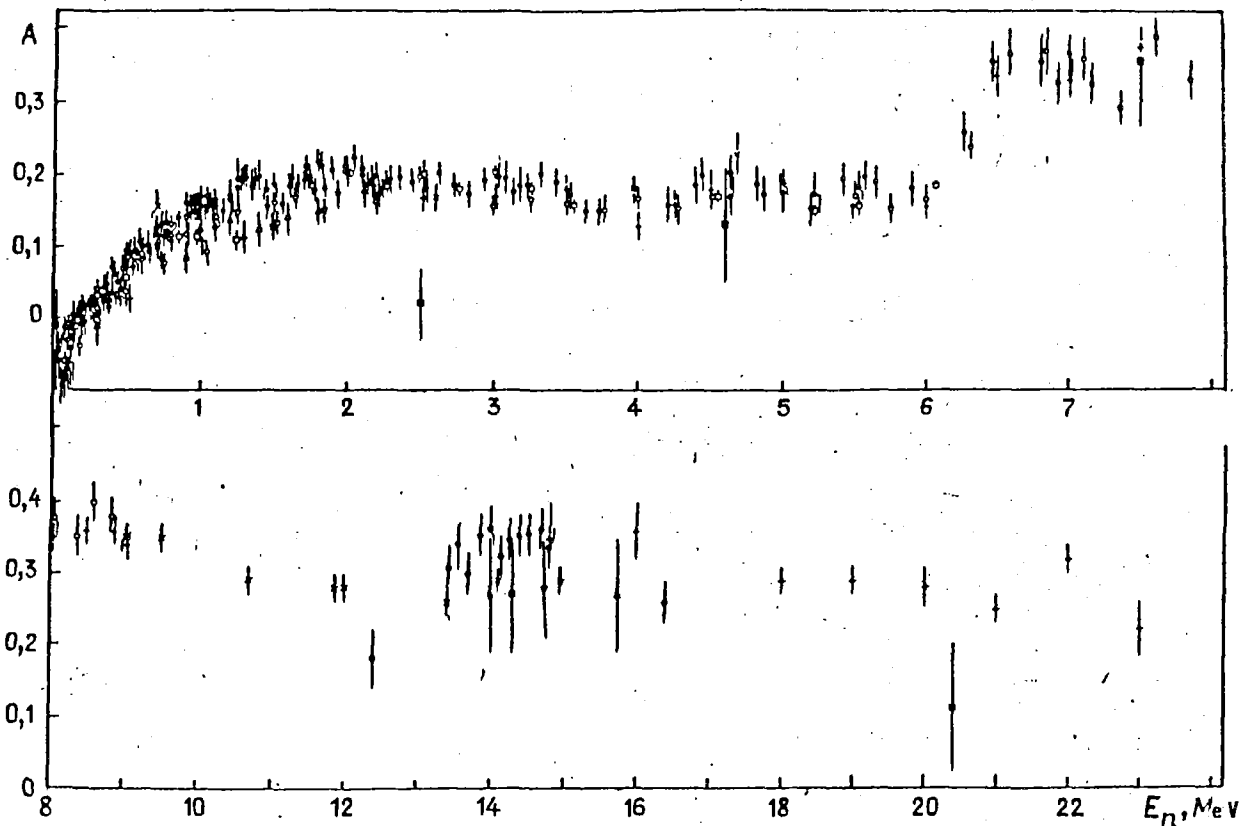
The angular anisotropy of ^{235}U fission fragments was studied with the use of glass detectors. The measurements were performed in the neutron energy range 0.014-7.15 MeV. The angular distribution was fitted by $\cos \theta$ quadratic dependence. The results are compared with the data of other authors.

Data on the angular anisotropy of fission fragments $A = W(0^\circ)/W(90^\circ) - 1$ is of considerable interest in the experimental study of fission cross-sections. These data are needed for evaluation and for introducing significant corrections in the measurement of fission cross-sections as a function of the angle of emission of fission fragments in relation to the direction of the flux of neutrons inducing the fission. Moreover, the energy dependence of the angular anisotropy coefficient of fission fragments on excitation energy is an important characteristic for the study of the quantum states at the saddle point of fissionable nuclei. ^{235}U is used to study the fission cross-sections by measuring the angular anisotropy coefficient. In practice, it is not the absolute values of the fission cross-sections for each fissionable element that are experimentally measured but their behaviour in relation to a chosen standard (in international practice ^{235}U).

At present, the literature contains a considerable number of experimental studies on the angular distributions of fragments of ^{235}U fission induced by neutrons in the 0-24 MeV range [1-13]. In spite of the comparatively good accuracy of the individual measurements, the divergences between the results of different authors are substantial. Special attention should be paid to the significant differences between the available data in the low-energy region.

The survey contained in Ref. [1] is the first attempt to review the status of the data obtained on the angular anisotropy of ^{235}U fission fragments. This work was based on a careful study of data published at various times. Moreover, it includes some new and still unpublished material and draws attention to the difference between the results of studies [11, 13] carried out recently for 0.3 and 0.7-1.9 MeV neutrons, respectively. The final result of Ref. [1] is the calculation, by the statistical theory [14, 15], of the angular anisotropy of fission fragments in the neutron energy region of up to 11 MeV.

In the present work we made a detailed study of the angular distributions of fission fragments for the ^{235}U nucleus in the 0-7.15 MeV neutron energy region. The measurements were carried out on the KG-2,5 cascade generator and EhG-1 accelerator using the T(p,n) and D(d,n) reactions on solid targets. The fission fragment detectors were cylindrical glasses. The experimental device was a modification of the multi-angle 4π -detector [16]. In the study of the detailed dependence of the fission fragment angular distributions for a sufficiently large number of angles (about 10) and the nuclei considered in the present work it is important to maintain the given geometry and especially the identical positioning of the glasses and the fissionable layers during the prolonged measurement process. For this purpose the working layer with the fissionable substance was securely fixed during the measurement time in a special thin-walled holder; therefore the removable glass detectors could only occupy,



Dependence of the angular anisotropy of ^{235}U on neutron energy. Data from studies: \square, \diamond - [2]; ∇ - [3]; $+$ - [4]; \times - [5]; \square - [6]; \odot - [7, 12]; \diamond - [8]; \blacktriangle - [9]; \triangle - [10]; ∇ - [11]; \circ - [13]; \bullet - present work

in relation to this holder (and consequently to the layer), a strictly defined position in all series of irradiations.

The experimental device permitted the simultaneous use of several holders fixed at specific angles to the accelerated particle beam. This enabled us to obtain duplicate data on fission fragment angular distributions for three isotopes at an angle of 15° to the accelerated particle beam and for four isotopes at 155° .

In this paper we give the measurement results for the distributions, at an angle of 155° to an accelerated proton beam, of ^{235}U fission fragments in the neutron energy region of up to 0.740 MeV during the irradiation of ^{235}U together with ^{233}U and ^{242}Pu and also for the distributions, at an angle of 15° to a beam of accelerated protons and deuterons, in the 0.48-7.15 MeV region during the irradiation of ^{235}U together with ^{236}U and ^{238}U (interval in the low-energy region 10-100 keV, energy resolution 10-30 keV).

The targets used in the experiment were constituted of 99.9% ^{235}U in the form of oxide layers on thin rectangular aluminium supports, 8 mm long and 9 mm wide, cut from layers of considerably larger dimensions. The inhomogeneity of the layers was estimated to be about 5%. As a result of direct measurements after evaluation and allowance for the contribution to fission by neutrons scattered in the structures of the experimental device, corrections were made for the background of the experimental room (about 2%) and the background of the (p,n) reaction on the structural materials of the target holder. It was established in the experiment that the (p,n) reaction

was substantial in the 2.1-3 MeV region, i.e. when the background neutrons (about 4%) had an energy of up to 0.7 MeV.

Particular attention was paid to the D(d,n) reaction neutron background caused by deuterons impinging on the molybdenum substrate of the neutron target. For this purpose we used samples identical to the neutron target without deuterium. In obtaining the fission fragment angular distributions we also made corrections for the non-uniform distribution of the neutron flux over the area of the layer (about 1%) and a correction rendered necessary by geometric factors and the inhomogeneity of the layer.

The experimental angular distributions taking into account angular resolution and motion of the centre of mass were processed by the method of least squares in order to find the angular anisotropy coefficient on the assumption that $W(\theta)/W(90^\circ) = Q_0 + Q_2\cos^2\theta + Q_4\cos^4\theta$ (see figure). It will be seen from the figure that the results of the present experiment are in relatively good agreement with the data of other authors in the the neutron energy regions 0.2-0.7 MeV and above 1.9 MeV. Some decrease in the negative angular anisotropy at 0.06-0.08 MeV approximately to -0.1 in this experiment can be attributed to the more careful measurements in this region and to the reduction in the amount of structural materials in the top part of the target holder by a factor of 4-5 in comparison with earlier studies [6, 7]. In the neutron energy region of 0.7-1.5 MeV a substantial discrepancy is observed between the results of the present experiment and the data of other studies [7, 10, 11, 13]. The greatest discrepancy is observed in studies [7, 10], which were performed earlier. The results of the two latest studies [11, 13] in this neutron energy region are substantially closer to the data of the present experiment. A more detailed analysis of the results obtained on the shape of the fission fragment angular distributions and the energy dependence of angular anisotropy lies outside the scope of the present experiment.

THE AVERAGE KINETIC ENERGY OF FISSION FRAGMENTS

V.G. Vorob'eva, B.D. Kuz'minov

The authors analysed experimental data on the mean kinetic energy of fragments for a fixed nucleonic structure and excitation energy of fissionable nuclei. The numerical data have been reduced to a single standard.

By now a sufficient volume of experimental data has been accumulated on the kinetic energies of fission fragments (spontaneous fission, thermal- and fast-neutron-induced fission, charged-particle-induced fission and photofission). The present material supplements the studies published earlier [1, 2]. In all the studies considered the fission fragments were recorded by semiconductor detectors, except in Ref. [3], where an ionization chamber was used for the purpose.

The greater part of the results on the kinetic energies of fragments were obtained in measurements using either ^{252}Cf spontaneous fission or ^{235}U thermal-neutron fission for calibration of the energy scale of fragments. Considering the convenience of work with californium targets and since ^{252}Cf spontaneous fission neutrons are used for standardizing the measurements of the average number of neutrons and the fission neutron spectra, the authors chose the value of the fragment kinetic energy in ^{252}Cf spontaneous fission for standardization of the data on the average kinetic energies of the fission fragments of various nuclei: $\bar{E}_k(^{252}\text{Cf}) = (186.3 \pm 1.0)$ MeV [1, 2]. As a supplementary standard the average kinetic energy of fragments during ^{235}U thermal neutron fission was taken: $\bar{E}_k(^{235}\text{U}) = (172.2 \pm 0.4)$ MeV. During thermal-neutron-induced fission of ^{235}U , ^{239}Pu and ^{241}Pu nuclei the

Table 1. Average kinetic energy of fragments during spontaneous fission

Fissionable nucleus	\bar{E}_k measured, MeV	Reduced to a single standard	Ref.
^{240}Pu	$177,25 \pm 0,30$	$180,41 \pm 0,30$	[4]
^{240}Pu	$177,30 \pm 0,20$	$177,10 \pm 0,20$	[5]
^{242}Pu	$180,16 \pm 0,20$	$179,96 \pm 0,20$	[6]
^{242}Pu	$180,03 \pm 0,09$	$179,83 \pm 0,09$	[7]
^{244}Pu	$182,0 \pm 1,0$	$181,80 \pm 1,0$	[7]
^{244}Pu	$180,8 \pm 0,30$	$183,96 \pm 0,30$	[8]
^{244}Cm	$181,7 \pm 1,0$	$181,50 \pm 1,0$	[9]
^{244}Cm	188,2	191,36	[10]
^{252}Cf	$186,25 \pm 1,2$	$181,41 \pm 1,2$	[10]
^{252}Cf	186,4	186,2	[11]
^{252}Cf	$181,25 \pm 1,3$	$184,41 \pm 1,3$	[12]
^{254}Fm	$195,1 \pm 1,0$	$194,9 \pm 1,0$	[13]
^{256}Cf	$187,2 \pm 0,9$	$187,6 \pm 0,9$	[14]
^{258}Md	$238 \pm 3,0$	$238,4 \pm 3,0$	[14]
^{259}Md	$200,7 \pm 1,4$	$203,86 \pm 1,4$	[15]
^{269}Fm	$242,0 \pm 6,0$	$245,16 \pm 6,0$	[16]
^{244}Fm	$196,0^*$	—	[17]
^{246}Fm	$198,7^*$	—	—
^{246}Fm	$196,4 \pm 4$	$199,56 \pm 4$	[18]
^{248}Fm	$195,6 \pm 4$	$198,66 \pm 4$	—

* The energy calibration of ionization chambers was performed with fragments of ^{235}U fission by thermal neutrons and also with induced ^{197}Au and ^{235}U fission by ^{12}C and ^{16}O ions. \bar{E}_k value for calibration reactions in Ref. [19].

Table 2. Average kinetic energy of fragments during fission by thermal neutrons

Fissionable nucleus	\bar{E}_k measured, MeV	Reduced to a single standard	Ref.
^{229}Th	$162,4 \pm 0,5$	$162,7 \pm 0,5$	[20]
^{231}Pa	$164,8 \pm 0,5$	$165,1 \pm 0,5$	[21]
^{232}U	$169,0 \pm 0,5$	$169,3 \pm 0,5$	[22]
^{233}U	$170,6 \pm 0,5$	$170,9 \pm 0,5$	[22]
^{235}U	$171,0 \pm 0,5$	$170,3 \pm 0,5$	[22]
^{235}U	$171,4 \pm 0,2$	$171,7 \pm 0,2$	[23]
^{237}Np	$170,7 \pm 0,7$	$171,0 \pm 0,7$	[23]
^{237}Np	$174,7 \pm 0,6$	$175,0 \pm 0,6$	[24]
^{238}Pu	$177,8 \pm 0,6$	$178,1 \pm 0,5$	[25]
^{239}Pu	$178,0 \pm 0,5$	$178,3 \pm 0,5$	[25]
^{239}Pu	176,57	178,73	[4]
^{239}Pu	$176,0 \pm 0,5$	$176,3 \pm 0,5$	[26]
^{239}Pu	$178,1 \pm 0,10^*$	$178,4 \pm 0,10$	[5]
^{241}Pu	$177,5 \pm 0,5$	$178,4 \pm 0,5$	[27]
^{241}Pu	$176,3 \pm 0,5$	$176,6 \pm 0,5$	[25]
^{241}Pu	$176,56 \pm 0,07$	$177,46 \pm 0,07$	[28]
^{241}Pu	$176,93 \pm 0,06$	$176,73 \pm 0,06$	[6]
^{241}Am	$179,7 \pm 0,4$	$180,0 \pm 0,4$	[29]
^{243}Am	$177,2 \pm 0,6$	$177,5 \pm 0,6$	[29]

* Statistical error.

recommended values of the average kinetic energy of fragments are (171.5 ± 0.3) , (178.6 ± 0.9) and (179.0 ± 0.6) MeV, respectively [1, 2]. Tables 1-8 give the results of measurement of the kinetic energies of fission fragments by different methods [3-37]. The data of all authors are reduced to a single standard.

Apart from studies with numerical data, there are experimental studies where the results are presented in the form of graphs [38-40].

Table 3. Average kinetic energy of fragments during neutron-induced fission of ^{232}Th

E_n , MeV	\bar{E}_k measured, MeV	Reduced to a single standard	Ref.	
1.36±0.02	163.28±0.13	163.58±0.13	[30]	
1.43±0.02	163.31±0.11	163.61±0.11		
1.60±0.02	163.22±0.07	163.62±0.07		
1.66±0.02	163.61±0.07	163.91±0.07		
1.72±0.02	163.36±0.07	163.66±0.07		
1.77±0.02	163.63±0.08	163.93±0.08		
1.86±0.02	163.27±0.07	163.57±0.07		
2.00±0.02	163.49±0.07	163.79±0.07		
2.20±0.02	163.38±0.06	163.68±0.06		
2.40±0.02	164.03±0.05	164.33±0.05		
2.96±0.02	164.19±0.06	164.49±0.06		
4.20±0.11	164.63±0.10	164.93±0.10		
5.30±0.11	164.87±0.06	165.17±0.06		
1.6 ^{+0.1} _{-0.13}	158.86±0.08	162.02±0.08		[31]
3.1±0.15	161.03±0.08	164.19±0.08		[32]
5.2±0.25	163.48±0.10	166.64±0.10		
1.32	162.10±0.10	162.40±0.10		
1.37	161.96±0.13	162.25±0.13		
1.42	162.52±0.10	162.52±0.10		
1.47	162.46±0.10	162.76±0.10		
1.62	162.60±0.10	162.60±0.10		
1.60	162.53±0.10	162.83±0.10		
1.60	162.70±0.10	163.01±0.10		
1.65	162.90±0.10	163.20±0.10		
1.70	162.93±0.10	163.23±0.10		
1.76	162.90±0.10	163.20±0.10		
1.86	162.78±0.10	163.08±0.10		
1.90	162.79±0.10	163.09±0.10		
1.96	162.92±0.10	163.22±0.10		
2.04	162.54±0.10	162.84±0.10		
2.14	162.99±0.10	162.69±0.10		
2.18	162.59±0.13	162.89±0.13		
2.24	162.96±0.10	163.26±0.10		
2.46	163.48±0.10	163.78±0.10		
2.59	163.75±0.13	164.05±0.13		
2.74	163.47±0.15	163.77±0.15		
3.14	163.77±0.15	164.07±0.15		
3.54	164.19±0.14	164.49±0.14		
5.78	164.49±0.18	164.79±0.18		

Table 4. Average kinetic energy of fragments during neutron-induced fission of ^{235}U

E_n , MeV	$\Delta\bar{E}_k$ measured, MeV	Reduced to a single standard	Ref.
0.179±0.024 ^{*2}	0.269±0.200 ^{*3}	172.469±0.200	[33] ^{*4}
0.298±0.024	0.073±0.200	172.273±0.200	
0.467±0.022	-0.063±0.200	172.147±0.200	
0.598±0.021	0.357±0.199	172.557±0.199	
0.748±0.020	0.326±0.200	172.526±0.200	
0.896±0.020	0.134±0.187	172.334±0.197	
1.046±0.020	0.484±0.197	172.654±0.197	
1.108±0.020	0.128±0.200	172.328±0.200	
1.459±0.034	0.267±0.143	172.467±0.143	
1.992±0.030	0.202±0.141	172.401±0.141	
2.491±0.028	0.042±0.146	172.242±0.146	
2.990±0.026	0.039±0.178	172.239±0.178	
3.254±0.047	0.026±0.219	172.226±0.219	
3.490±0.024	0.160±0.178	172.360±0.178	
3.760±0.044	-0.034±0.221	172.166±0.221	
3.964±0.024	0.017±0.178	172.217±0.178	
4.274±0.041	-0.020±0.221	172.160±0.221	
4.514±0.040	-0.432±0.221	171.768±0.221	
5.19±0.14	-0.860±0.292	171.350±0.292	
5.45±0.13	-0.469±0.264	171.731±0.264	
5.76±0.11	-0.644±0.256	171.556±0.256	
6.04±0.10	-1.045±0.240	171.155±0.240	
6.31±0.09	-0.575±0.241	171.625±0.241	
6.68±0.08	-0.833±0.256	171.367±0.256	
6.84±0.08	-1.012±0.245	171.186±0.245	
7.10±0.08	-0.663±0.231	171.537±0.231	
7.36±0.08	-1.363±0.228	170.837±0.228	
7.61±0.08	-0.756±0.216	171.444±0.216	
7.86±0.07	-0.925±0.218	171.275±0.218	
8.12±0.07	-0.515±0.207	171.655±0.207	
8.36±0.07	-0.930±0.204	171.270±0.204	
8.58±0.07	-0.695±0.202	171.505±0.202	
8.83±0.07	-0.707±0.192	171.493±0.192	
0.50±0.08	170.40±0.15	172.21±0.15	
	(170.35±0.05)	(172.15±0.05)	
5.55±0.25	169.55±0.22	171.35±0.22	
	(169.42±0.07)	(171.22±0.07)	

* $\Delta\bar{E}_k = \bar{E}_k(E_n) - E_n(\text{therm})$, where $E_n(\text{therm}) = 170.0$ MeV.

² Resolution (FWHM).

³ Statistical error.

⁴ In Ref. [33] measurements were performed by two methods: measurements of two fragment velocities and measurements of two fragment energies. The kinetic energy values obtained by measuring the energy of fragment pairs are given in brackets.

Table 5. Average kinetic energy of fragments during neutron-induced ^{235}U fission [32]

E_n , KeV	\bar{E}_K measured, KeV	Reduced to a single standard
0,61	172,34±0,20	172,64±0,20
0,72	172,45±0,10	172,75±0,10
0,82	172,09±0,12	172,39±0,12
0,93	172,00±0,10	172,30±0,10
1,04	172,18±0,10	172,48±0,10
1,14	172,53±0,10	172,83±0,10
1,35	172,56±0,10	172,88±0,10
1,55	172,44±0,10	172,74±0,10
1,75	172,38±0,10	172,68±0,10
1,95	172,44±0,10	172,74±0,10
2,16	172,18±0,10	172,48±0,10
2,36	172,81±0,10	173,11±0,10
2,54	172,20±0,10	172,50±0,10
2,75	172,04±0,10	172,34±0,10
2,96	172,06±0,10	172,36±0,10
3,16	172,14±0,10	172,44±0,10
3,34	172,20±0,10	172,50±0,10
3,54	171,95±0,10	172,25±0,10
3,50	172,00±0,10	172,30±0,10
3,98	172,02±0,10	172,32±0,10
4,46	171,54±0,10	171,84±0,10
4,80	171,79±0,10	172,09±0,10
5,12	171,90±0,10	172,20±0,10

Table 6. Total kinetic energy in ^{239}Pu resonances [5]

E_n , eV	E_K measured, KeV	Reduced to a single standard
7,82	178,13±0,07*	177,93±0,07
10,93	178,00±0,07	177,80±0,07
11,89	178,06±0,13	177,86±0,13
14,31	178,06±0,09	177,86±0,09
14,68		
15,46	178,01±0,18	177,81±0,18
17,66	178,10±0,13	177,90±0,13
26,24	177,93±0,16	177,73±0,16
32,31	178,21±0,26	178,01±0,26
41,5*2	177,97±0,10	177,77±0,10
47,6	177,79±0,21	177,59±0,21
60,0*2	178,06±0,13	177,86±0,13
57,44	178,02±0,14	177,82±0,14
59,22	178,00±0,19	177,80±0,19
66*2	178,04±0,10	177,84±0,10
75*2	177,99±0,12	177,79±0,12
85*3	178,26±0,12	178,06±0,12

* Statistical error.
*2 Insufficient separation of resonances.
*3 Statistical error and insufficient separation of resonances.

Table 7. Average kinetic energy of fragments during charged-particle induced fission

Target nucleus	Particle	Particle energy, KeV	\bar{E}_K measured, KeV	Chosen standard \bar{E}_K (^{252}Cf)	Reduced to a single standard	Ref.
^{248}Cm	^{18}O	95,0	234±2,0	183,14	237,16±2,0	[34]
^{256}Fm	^{18}O	95,0	238±3,0		241,16±3,0	
^{260}Fm	^{18}O	95,0	242±6,0		245,16±6,0	
^{233}U	(d, pf)	13,5	171,62±1,0	183,14	174,65±1,0	[35]
^{260}Cf	(t, pf)	$4,4 < \bar{E}_K < 9,8$	189,1	183,14	192,26	[1]

Table 8. Average kinetic energy of fragments during photofission

Target nucleus	Photon energy, MeV	E_K measured, MeV	Chosen standard E_K (^{252}Cf)	Reduced to a single standard	Ref.
^{235}U	26,0	$170,6 \pm 2,0$	183,14	$173,16 \pm 2,0$	[36]
^{238}U	26,0	$170,9 \pm 2,0$	183,14	$174,06 \pm 2,0$	[37]
^{238}U	12	$171,76 \pm 0,56$		$174,94 \pm 0,56$	
	15	$171,4 \pm 0,13$		$174,57 \pm 0,13$	
	20	170,88		174,04	
	30	$170,37 \pm 0,26$		$173,53 \pm 0,26$	
	70	$169,41 \pm 0,30$		$172,57 \pm 0,30$	
^{240}Pu	12	$173,89 \pm 0,24$	183,14	$177,15 \pm 0,24$	[4]
	15	$173,25 \pm 0,24$		$176,41 \pm 0,24$	
	20	$172,46 \pm 0,20$		$175,62 \pm 0,20$	
	30	$172,22 \pm 0,31$		$175,38 \pm 0,31$	
^{242}Pu	12	$174,34 \pm 0,12$	179,6 (^{241}Pu)	$178,74 \pm 0,12$	[8]
	15	$173,59 \pm 0,15$		$172,99 \pm 0,15$	
	20	$173,07 \pm 0,10$		$172,47 \pm 0,10$	
	30	$172,86 \pm 0,17$		$172,26 \pm 0,17$	
^{244}Pu	12	$173,58 \pm 0,40$	179,6 (^{241}Pu)	$172,98 \pm 0,40$	[8]
	15	$172,59 \pm 0,22$		$171,99 \pm 0,22$	
	20	$171,91 \pm 0,20$		$171,31 \pm 0,20$	
	30	$171,63 \pm 0,26$		$171,06 \pm 0,26$	

THE DEPENDENCE OF THE FISSION CROSS-SECTIONS FOR HEAVY
NUCLEI ON NEUTRON ENERGY IN THE "PLATEAU" REGION

G.N. Smirenkin, B.I. Fursov

The paper presents a wide set of experimental data on fission probability and fast neutron cross-sections for Pa-Cf nuclei in the first "plateau" region ($E_n = 1-7$ MeV). Energy dependences of fission cross-sections, fission probabilities and compound nucleus formation cross-sections are compared. Some conformity to natural laws regarding fission probability energy dependence as a function of nucleon composition is identified.

Fission of heavy nuclei in the reaction (n,f) is characterized by the presence of a "plateau" region in the fission cross-section which is a function of neutron energy. This property of the fission cross-sections $\sigma_f \sim \sigma_c \Gamma_f / (\Gamma_f + \Gamma_n)$ can be explained by the weak dependence on E_n of the values contained in this equation: the compound nucleus formation cross-sections σ_c and the width ratios (neutron and fission) of its predominant decay processes Γ_n / Γ_f [1]. The concept "plateau" in the dependence $\sigma_f(E_n)$ is approximate as is the assumption $\sigma_c = \text{const}$ and $\Gamma_n / \Gamma_f = \text{const}$. However, the latter is often used not only for the sake of simplicity but also because of the lack of system in the available knowledge about the energy dependence of the registered values, particularly of the ratio Γ_n / Γ_f . This is the actual situation, despite the urgent practical requirements for accuracy in the measurement and description of nuclear physics constants, of which the dependence $\sigma_f(E_n)$ is one of the most important.

In this work an attempt is made, using the results of multiple measurements of cross sections for the fission of heavy nuclei by fast neutrons in electrostatic generators [2], to generalize the data obtained and to deduce the basic principles governing the dependence $\sigma_f(E_n, Z, N)$ for the first "plateau" region ($2 \lesssim E_n \lesssim 5$ MeV).

Experimental data on the dependence $\sigma_f(E_n)$ (Fig. 1) are obtained from direct measurements of the fission cross-section ratios. For standard cross-sections (^{235}U and ^{239}Pu), evaluation data from the ENDF/B-V library were used. The set of nuclei studied by us was supplemented by the results of similar measurements for ^{234}U [3], ^{244}Pu [4], ^{238}Pu [5], $^{242}\text{Am}^m$ and ^{245}Cm [6]. From Fig. 1 it can be seen that the data of other authors have on average a wide spread which is disadvantageous for the study of such regular properties as the fission cross-section "plateau" and such minor effects as their deviation from the traditional simplifying assumptions $\sigma_f = \text{const}$ and $\Gamma_n / \Gamma_f = \text{const}$.

From the experimental data it can be seen that the virtually ideal "plateau" $\sigma_f(E_n) \approx \text{const}$ in the $^{238}\text{U}(n,f)$ reaction, which was widely used previously [1] to demonstrate this property is in fact untypical for the pattern of measurements observed for $\sigma_f(E_n, Z, N)$. However, the presence in the same energy region $E_n \approx 2-5$ MeV of a monotonous (near to linear) dependence $\sigma_f(E_n)$ is characteristic of this pattern and makes it possible to judge the gradient of the "plateau" which, as can be seen from Fig. 1, depends to a large extent on the nucleonic composition of the nucleus: on the parity of the number of nucleons and also generally on the numbers Z and N . Some of these effects were noted in Ref. [7].

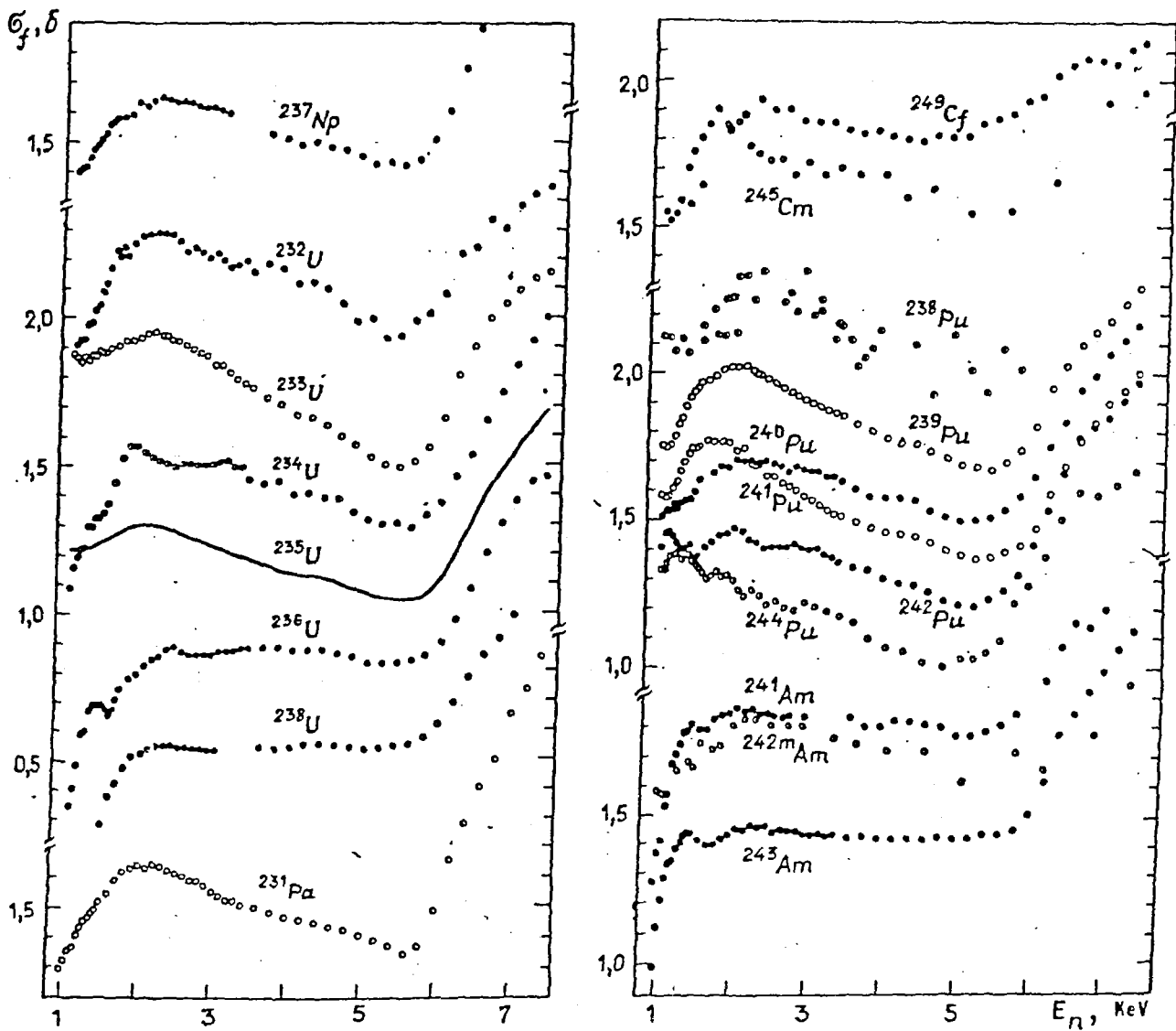


Fig. 1. Dependence of fission cross-sections on neutron energy. Data from the present work and Ref. [2]: \circ - N-even target nuclei, \bullet - N-odd target nuclei. Data from Refs: \circ - [3] for ^{234}U , [4] for ^{244}Pu , [5] for ^{238}Pu (up to 6 MeV), [6] for $^{242}\text{Am}^m$ and ^{245}Cm .

The fissionability of the nuclei $P_f(E_n)$. In order to discuss the properties $d\sigma_f/dE_n$ it is necessary to separate the effects caused by the energy dependence of the characteristics σ_c and Γ_n/Γ_f determining the dependence $\sigma_f(E_n)$. For this purpose, unlike in the case of the dependence $\sigma_f(E_n)$, consideration is usually given to the fissionability of the nuclei

$$P_f(E_n) = \frac{\sigma_f(E_n)}{\sigma_c(E_n)} \approx (1 + \Gamma_n/\Gamma_f)^{-1},$$

having a weak dependence on the properties of the entrance channel of the reaction and essentially determined by the competition of the basic decay channels of the compound nucleus (neutron and fission).

Figure 2 shows the results of calculation for the dependence $\sigma_c(E_n)$ using the coupled-channel method, carried out in Ref. [8], for

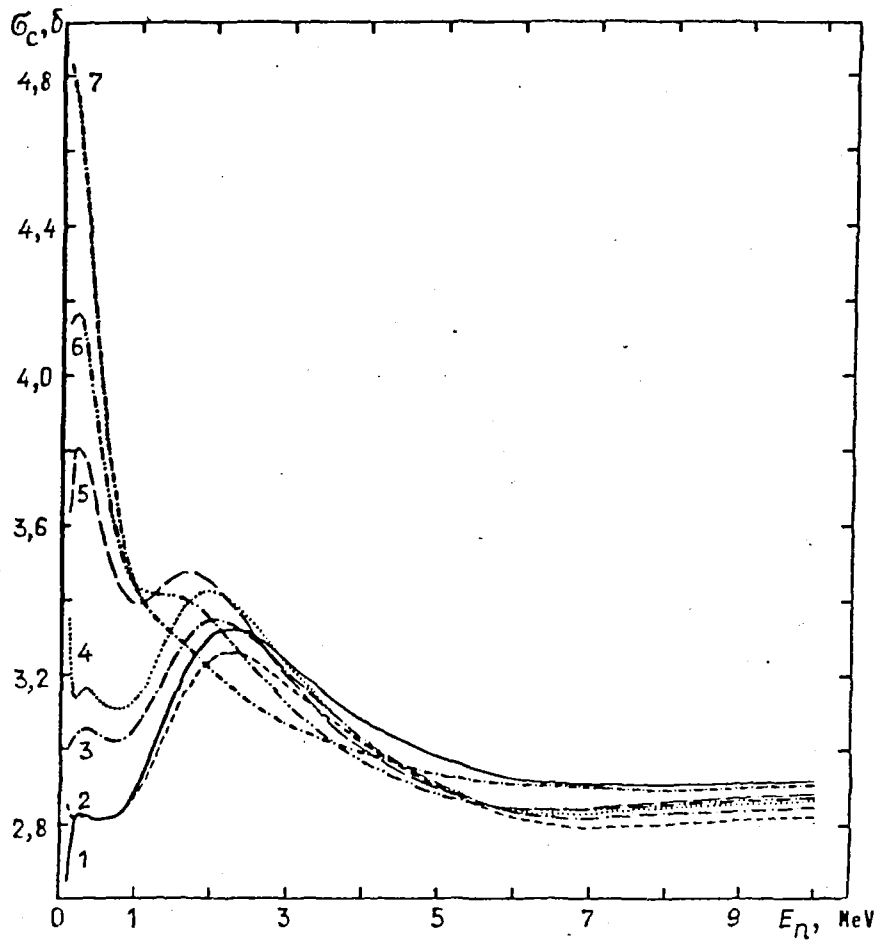


Fig. 2. Dependence of the cross-section compound nucleus formation on neutron energy. [8]: 1 - ^{230}Th ; 2 - ^{232}Th ; 3 - ^{234}U ; 4 - ^{238}U ; 5 - ^{242}Pu ; 6 - ^{246}Cm ; 7 - ^{252}Cf

the wide range of nuclei from ^{230}Th to ^{252}Cf . From these it can be seen that the dependence $\sigma_c(E_n, Z, N)$ is fairly strong but the effect of individual properties of the nuclei quickly decreases as the neutron energy changes. In the region $E_n > 2$ MeV the curves are contained in a fairly narrow corridor, the width of which is a few per cent of σ_c . Nevertheless, in determining the fissionability of nuclei the ratio $\sigma_c(E_n)$ is adopted for one of the nearest neighbours in terms of the Z and N numbers.

Data on the fissionability of the nuclei $P_f(E_n)$ is shown in Fig. 3. The behaviour of fissionability with change in energy can approximately be described by the linear dependence

$$P_f(E_n) = P_f(E_n^0) + \frac{dP_f(E_n^0)}{dE_n} (E_n - E_n^0).$$

The values $P_f(E_n^0)$ and $dP_f(E_n^0)/dE_n$, evaluated in the range $E_n = 2.5-4.5$ MeV ($E_n^0 = 3.5$ MeV) are shown in the table. At lower energies, the dependence $P_f(E_n)$ changes more sharply, sometimes irregularly, which is characteristic of the region close to one of the thresholds of the competing processes - fission or neutron emission. At $E_n > 4.5$ MeV this dependence systematically "sags" by an average of 5% ($E_n = 5.5$ MeV). In most cases this conditioning effect is associated with inaccuracy in the value $\sigma_c(E_n)$ [10] at $E_n > 4.5$ MeV, since it does not occur in the fissionability energy dependence directly measured in direct reactions.

Table. Fissionability characteristics of nuclei

Isotope	P_f	dP_f/dE_n	$P_f^{-1} dP_f/dE_n$	$P_f^{-1} (1-P_f^{-1}) dP_f/dE_n$
		MeV ⁻¹		
²³¹ Pa	0,38	-0,012	-0,036	-0,054
²³² Pa	0,70	-0,007	-0,010	-0,033
²³³ Pa	0,57	-0,020	-0,035	-0,081
²³⁴ U	0,47	+0,004	+0,009	+0,016
²³⁵ U	0,38	-0,006	-0,016	-0,026
²³⁶ U	0,28	+0,016	+0,057	+0,079
²³⁸ U	0,173	+0,012	+0,069	+0,084
²³⁷ Np	0,50	+0,006	+0,012	+0,024
²³⁸ Pu	0,69	+0,014	+0,020	+0,065
²³⁹ Pu	0,59	+0,003	+0,005	+0,012
²⁴⁰ Pu	0,52	+0,006	+0,012	+0,024
²⁴¹ Pu	0,49	-0,004	-0,008	-0,016
²⁴² Pu	0,44	0,000	0,000	0,000
²⁴⁴ Pu	0,38	-0,007	-0,018	-0,030
²⁴¹ Am	0,59	+0,033	+0,056	+0,136
^{242m} Am	0,57	+0,022	+0,038	+0,090
²⁴³ Am	0,47	+0,024	+0,051	+0,096
²⁴⁵ Cm	0,56	+0,005	+0,009	+0,020
²⁴⁹ Cf	0,61	+0,001	+0,002	+0,004

Since the fissionability of various nuclei differs by several factors, the energy dependence $P_f(E_n)$ can be conveniently characterized by the relative quantity $P_f^{-1}(dP_f/dE_n) = d(\ln P_f)/dE_n$, which is also given in the table. From the data given, it follows that the relative changes in $P_f(E_n)$ are at a maximum for those target nuclei whose cross-sections have a more perfect "plateau" (²³⁸U, ²⁴¹Am, ²⁴³Am). Thus, the "plateau" in the dependence $\sigma_f(E_n)$ does not prove the approximate constancy of the ratio Γ_n/Γ_f , but on the contrary is a consequence of the very strong dependence of that ratio (in the case of the nuclei studied) and this dependence leads to contradictory and somewhat similar changes in the factors σ_c and P_f .

The energy dependence $P_f(E_n)$ and the nucleonic composition of the nucleus. The primary characteristic determining the probability of fission is the ratio of the mean widths Γ_n/Γ_f . Its relative change can be expressed through the fissionability parameters

$$\frac{d \ln \Gamma_n / \Gamma_f}{dE_n} = P_f^{-1} (1 - P_f)^{-1} dP_f / dE_n.$$

The values of the right-hand side of this equation calculated for $E_n = E_n^0$ are given in the table and in Fig. 4.

The following conclusions can be drawn from the data examined:

1. The fissionability energy dependences and the ratio Γ_n/Γ_f are associated with even-odd differences: target nuclei with an even

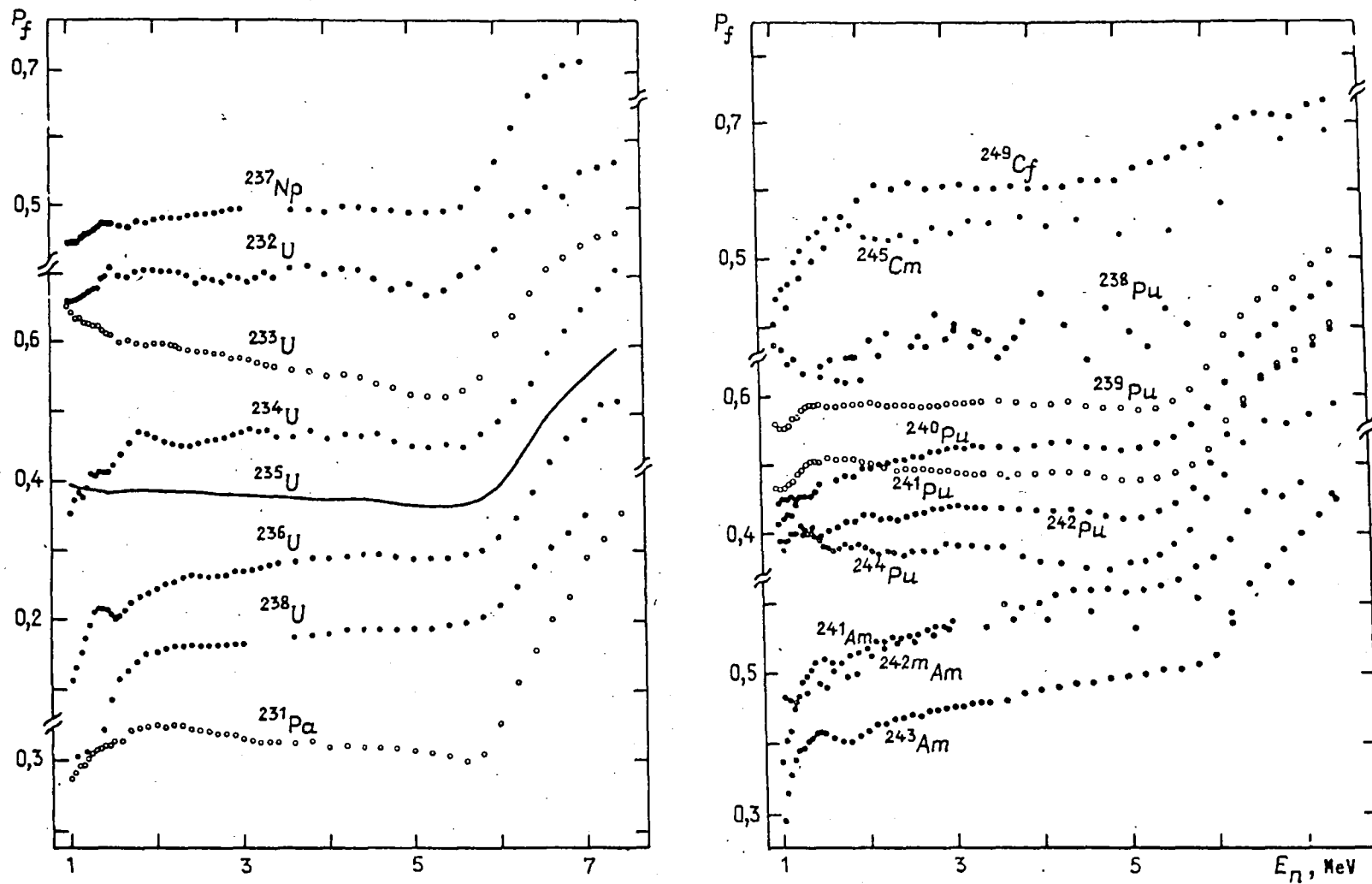


Fig. 3. Dependence of the fissionability of nuclei P_f on neutron energy E_n . Data from the present work and Ref. [2] ● - N-even target nuclei; ○ - N-odd target nuclei. Data from Refs: ● [3] for ^{234}U , [4] for ^{244}Pu , [5] for ^{238}U (up to 6 MeV), [6] for ^{242}Am and ^{245}Cm

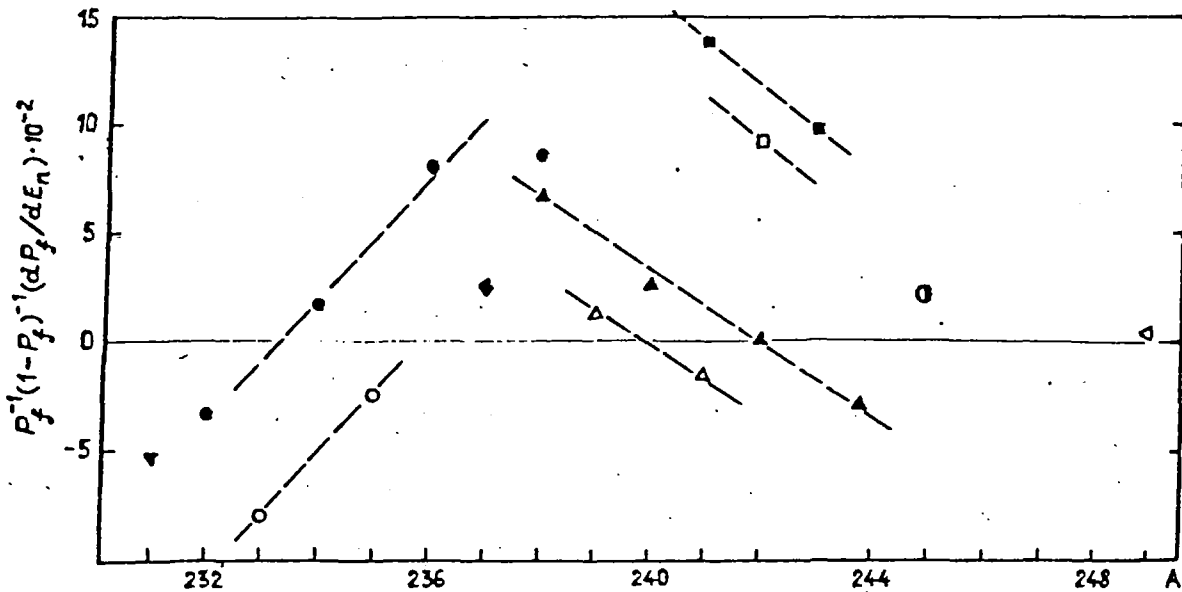


Fig. 4. Dependence of the parameter $P_f^{-1}(1-P_f)^{-1}dP_f/dE_n$ on the mass number of the target nucleus. Dark marks for N-even nuclei, light marks for N-odd: ∇ - palladium; \circ, \bullet - uranium; \blacklozenge - neptunium; Δ, \blacktriangle - plutonium; \square, \blacksquare - americium; \bullet - curium; \triangleleft - californium.

number of neutrons, shown in Fig. 4 by black marks, are characterized by large values for dP_f/dE_n and other parameters (see table). The insensitivity, noted earlier [1 and 9]), of the values P_f and Γ_n/Γ_f (for the middle of the "plateau" $E_n \approx E_n^0$) to even-odd variations in the nucleonic composition of the nuclei is a result of the smallness of the ratio dP_f/dE_n in general and the change in the N number by one in particular in comparison with the average ratios dP_f/dN and dP_f/dZ ;

2. The value $P_f^{-1}(1-P_f)^{-1}dP_f/dE_n$ increases as the number N increases for identical parity of uranium isotopes but falls for plutonium isotopes and, it appears, for americium isotopes also. There are not enough neutron data available to produce representations of the Z-dependence.

The theoretical description of the fission cross-sections and fissionability of actinides in the energy range examined constitutes a difficult task which involves taking numerous factors into account: the two-humped shape of the fission barrier, the influence of shell structure and of collective excitations, the effects of coupling of nucleons on level density, the difference in the properties of the excited nuclei in equilibrium and transient states, and so on. Taking each of these into account may have a significant bearing on the effect which is being studied experimentally by the authors. In such a situation an attempt to make a qualitative interpretation on the results of this work would be somewhat hazardous.

The difficulties of producing a theoretical description of the dependences $\sigma_f(E_n)$ and $P_f(E_n)$ underline the importance of classifying these characteristics. The scale of the effect $P_f^{-1}dP_f/dE_n \approx 7 \times 10^{-2} \text{ MeV}^{-1}$ evaluated by the authors indicates that the classification developed earlier [10] on the assumption $P_f(E_n) = P_f(E_n^0) = \text{const}$ can predict the fission cross-sections $\sigma_f(E_n)$ with an accuracy of better than $\pm 20\%$. This accuracy is established on the basis of the requirements for nuclides with which it is difficult or impossible to carry out direct experiments because their lifetime

is too short for measurements to be taken. The authors hope that the establishment of representations of the dependence dP_f/dE_n on the Z and N numbers, on which a start has been made in the present study, will be continued with the help of data on fissionability in direct reactions and that on this basis it will be possible to obtain new data about the phenomenological description of fission cross-sections and the fissionability of heavy nuclei.

EVALUATION OF THE ENERGY DEPENDENCE OF THE AVERAGE NUMBER OF
PROMPT NEUTRONS $\bar{\nu}_p$ FOR NEUTRON-INDUCED FISSION OF
 ^{235}U IN THE 0-20 MeV ENERGY RANGE

V.V. Malinovskij, M.S. Tarasko

The most detailed sets of $\bar{\nu}_p$ were used for the evaluations, and the necessary corrections made. The least-squares fitting procedure was applied for each data set to derive segmented straight lines. The final estimates were made by the method of least squares, including systematic experimental errors. The results of this study are compared with other evaluations.

The average number of prompt neutrons $\bar{\nu}_p$ for the fission of ^{235}U nuclei was measured with the use of monoenergetic neutrons and not less than four experimental values [1-23] (Table 1). For practical purposes, it is necessary to have an evaluated dependence which can be used to calculate the value and uncertainty of the number of $\bar{\nu}_p$ for an arbitrary neutron energy E_n . To this end, we chose a piecewise linear dependence which takes into account that the evaluated value of $\bar{\nu}_p$ is determined at different sectors of the 0-20 MeV range by the fission of compound nuclei differing in excitation and nucleonic composition and by the contribution of inelastically scattered neutrons from the $(n, xn'f)$ reactions (x equals 1, 2, 3). The true dependence $\bar{\nu}_p(E_n)$ is undoubtedly more complex than the piecewise linear dependence but the present status of experimental data for neutron energies above 6-7 MeV will hardly enable us reliably to determine a more complex dependence. The evaluation method is described in detail in Ref. [24]. The systematic errors attributed to each data set are given in Table 1. The data used are normalized in accordance with the values of the average number of prompt neutrons for ^{252}Cf spontaneous fission, equal to 3.757 ± 0.005 and with the values for thermal neutron fission of ^{235}U , equal to 2.411 ± 0.005 , taken from Ref. [25].

Table 2 gives the evaluated values of $\bar{\nu}_p$ for neutron-induced fission of ^{235}U . The value of χ^2 and the number of degrees of freedom correspond to the number of parameters obtained from individual data sets. The uncertainty of the standard was taken into account by multiplying all the fitting errors by $(1 + \sigma_{st}^2/\sigma_{fit}^2)^{1/2}$, where $\sigma_{st} = 0.005$ and σ_{fit} is the smallest of the fitting errors.

In Fig. 1 we show the results of studies published (or corrected [11, 13-15]) after 1972. The systematic errors in studies published up to 1970 are slightly higher in comparison with those of the authors. The 1969 [11] data corrected in Ref. [10] were renormalized once more in accordance with the refined results of the same authors [16, 17]. Of the 33 values given in Ref. [19], only 28 (up to neutron energies of 10 eV) were used; the remaining values were clearly erroneous. According to a later communication of the same authors [26] the results of Refs [19, 20] were reduced by 25% (systematic shift due to the use of different fission chambers with a ^{252}Cf layer). This correction minimizes the divergence in the results of measurements of $\bar{\nu}_p$ for thermal neutrons revised with allowance for the correction for the thickness of the fissionable material layer in Ref. [23].

Only two data sets [12, 22] have been published for neutron energies above 15 MeV. The results of Ref. [22] were taken into account with a large systematic error since the normalization of detector efficiency performed by the authors is not very reliable. The data of Refs [12, 22] differ

Table 1. Set of experimental data used in the evaluation of \bar{v}_p for neutron-induced fission of ^{235}U

Neutron energy range, MeV	Number of experimental points	Standard used \bar{v}_p (^{235}U)	Type of neutron detector	Systematic error taken in evaluation, %	Reference
0,03-1,76	6	2,414 [\bar{v}_p (^{235}U)]	$^{10}\text{BF}_3$ counters in moderator	0,8	(1)
0,28-14,6	6	3,771	Large liquid scintillator (LLS)	1,1	(2)
0,04-7,96	18	3,782	LLS	1,2	(3)
0,101-2,572	9	3,76	Boron tank	0,8	(4)
0,039-1,0	16	3,782	$^{10}\text{BF}_3$ counters in moderator	0,8	(5)
0,37-3,25	14	2,414	Same	1,5	(6)
0,66-6,60	37	3,772	LLS	1,1	(7)
0,0-1,515	13	3,782	^3He counters in moderator	0,9	(8)
0,198-0,986	34	3,756	LLS	0,7	(9)
1,87-14,79	22	3,782	"	0,65	(10, 11)
22,79-28,28	8	3,782	"	0,7	(12)
0,0-1,9	15	3,745	"	0,56	(13-15)
0,21-1,87	41	3,745	"	0,61	(16, 17)
0,88-5,73	15	3,756	"	1,12	(18)
(0,005-60) $\cdot 10^{-6}$	28 (33)*	1	"	0,29	(19)
$6 \cdot 10^{-4}$ -11,12	20	-	"	0,68	(20)
1,14-14,66	29	3,732	"	0,69	(21)
17-26,9	4*2	*3	Neutron multiplier (^{235}U) and scintillator	2,76	(22)
$< 8 \cdot 10^{-8}$	From five measurements	-	LLS and boron tank	0,12*4	(23)

* The last five values of this measurement series were not considered since they are known to be erroneous.
 *2 Of the whole set of measurements [22], only four values were used in this range.
 *3 The detector efficiency was normalized by comparing the results of measurement of \bar{v}_p for energies below 15 MeV with the evaluated data of Ref. [27].
 *4 The weighted mean value of the results of measurement for thermal neutrons.

Table 2. Evaluation of the energy dependence of \bar{v}_p for neutron-induced fission of ^{235}U

Parameter	Neutron energy, MeV						
	$2,53 \cdot 10^{-8}$	0,1	1,3	3,6	7,0	14,0	20,0
Value of \bar{v}_p	2,408	2,424	2,543	2,825	3,384	4,426	5,078
Error:							
Obtained during fitting	0,004	0,006	0,007	0,013	0,011	0,016	0,016
With allowance for standard error	0,005	0,008	0,009	0,016	0,014	0,021	0,021
Correlation matrix	1						
	-0,01	1					
	0,00	-0,37	1				
	0,00	0,07	-0,19	1			
	0,00	0,00	0,00	-0,01	1		
	0,00	0,00	-0,01	0,00	-0,19	1	
	0,00	0,00	0,00	0,00	-0,10	0,50	1

Remarks: $\chi^2 = 55.3$ for 52 degrees of freedom.

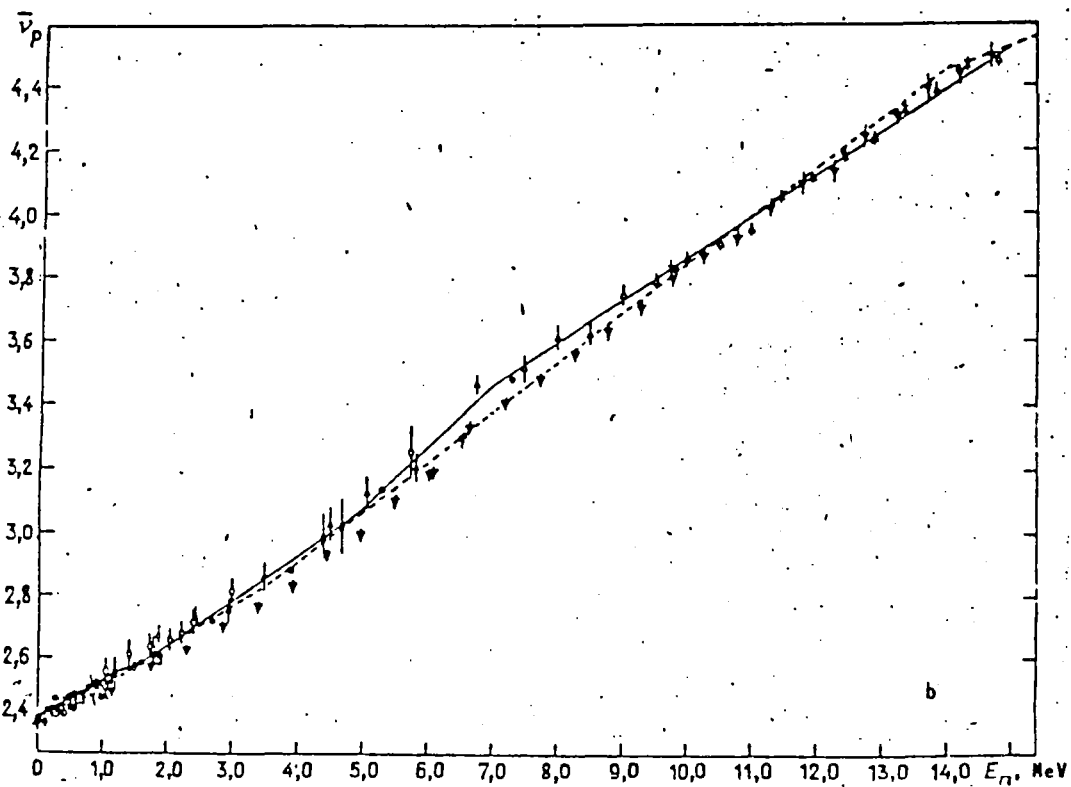
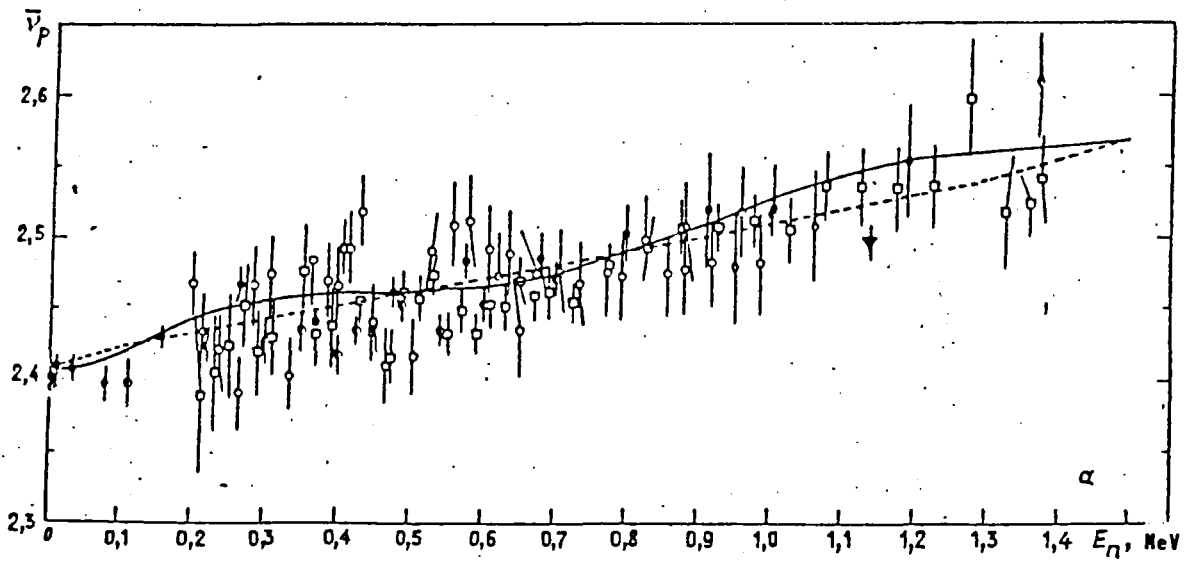


Fig. 1. Dependence of $\bar{\nu}_p$ on neutron energy for the fission of ^{235}U nuclei in the 0-1.5 MeV (a) and 0-15 MeV (b) ranges. Experimental data from Refs: \circ - [9]; Δ - [10, 11]; \odot - [13-15]; \diamond - [18]; \bullet - [20]; ∇ - [21]; \square - [16, 17]. Evaluated data from Refs: — - [27]; - - - present study.

substantially (up to 5-6%). The actual error in evaluation of the average number of ν_p in the 20 MeV region is therefore about 4%.

Table 2 and Figs 1 and 2 give the evaluation results. The data used agree satisfactorily. As will be seen from the figures, the structure revealed in the evaluation [27] is, in our opinion, not justified. The difference in the evaluations does not exceed 1% except in the region near 20 MeV.

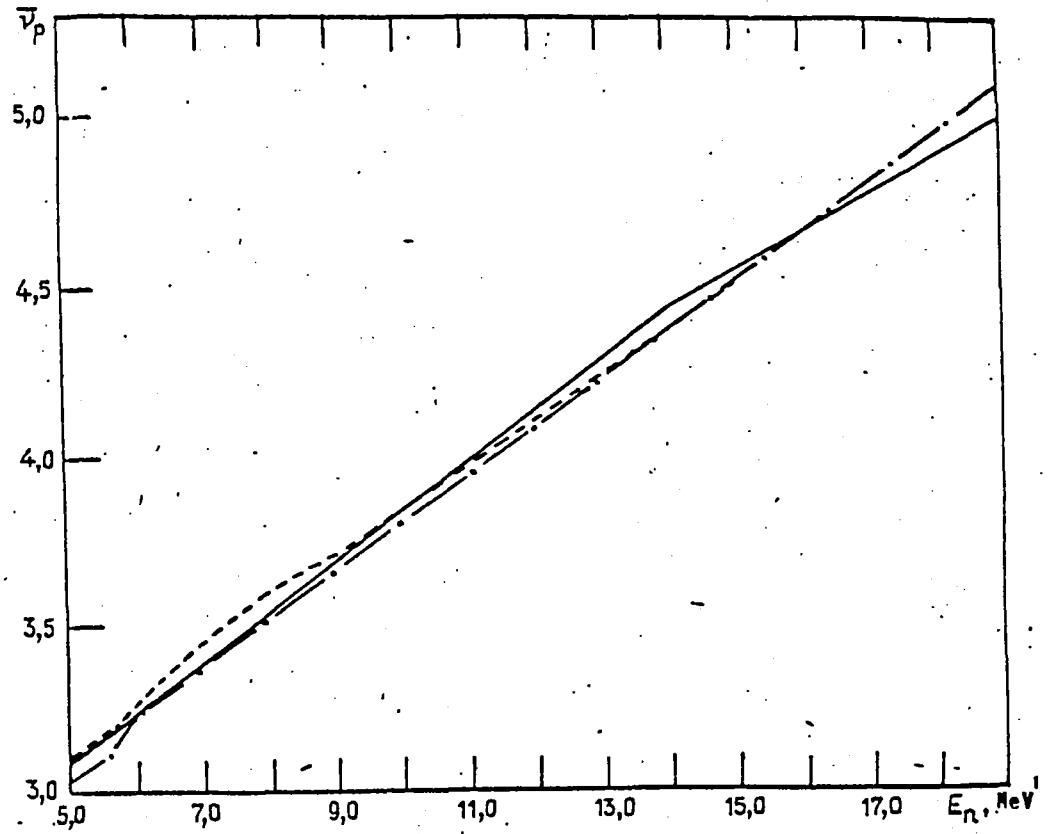
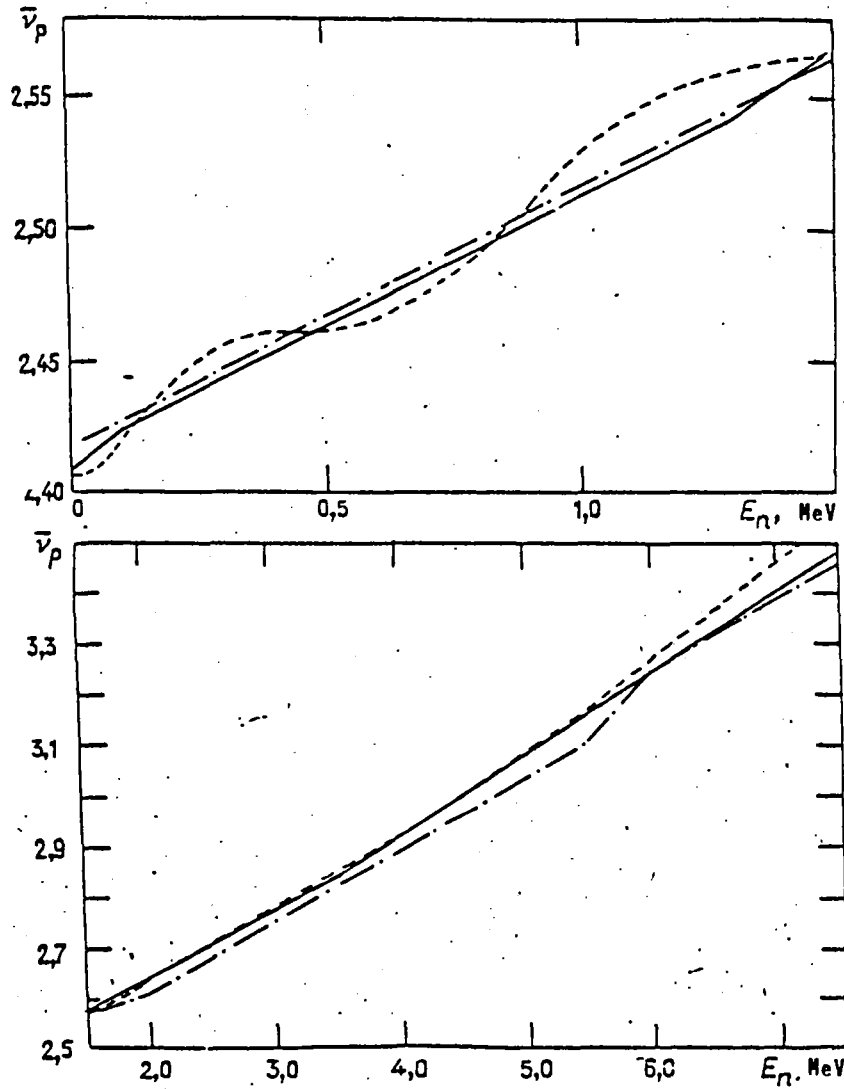


Fig. 2. Comparison of the results of evaluation of the dependence of $\bar{\nu}_p$ on neutron energy in various ranges.
 Evaluated data from Refs: --- [27]; - · - · - [28] (ENDF/B-V);
 ——— present study.

THE EXPERIMENTAL DETERMINATION OF RESONANCE SELF-SHIELDING FACTORS
AFFECTING THE NEUTRON RADIATIVE CAPTURE CROSS-SECTION FOR ^{238}U
IN THE 10 TO 140 keV ENERGY RANGE

V.N. Kononov, E.D. Poletaev, M. V. Bokhovko, L.E. Kazakov,
V. M. Timokhov, A.A. Voevodskiy

A method for experimental determination of capture self-shielding factors is described, based on simultaneous measurement of the transmission and the capture self-indication. The measurements were carried out with the EG-1 FEH1 pulsed Van de Graaff accelerator using the time-of-flight technique. The results obtained are in agreement with the data for the group constants BNAB.

High standards of accuracy are required for the measurement of neutron data used for fast-neutron reactor calculations (2.5-3% over a wide energy range, in the case of the ^{238}U neutron radiative capture cross-section). The same degree of accuracy should clearly apply to determination of the resonance self-shielding factors used to calculate the resonance structure of neutron cross-sections. However discrepancies in both experimental data on the resonance self-shielding factors affecting the capture cross-section [1-3] and the results of their calculation using mean resonance parameters [4] exceed this value significantly for several energy groups.

This experiment is a continuation of earlier work [1, 5, 6] on the measurement of resonance self-shielding factors for the neutron capture cross-section in ^{238}U , using a neutron spectrometer with the EG-1 FEH1 pulsed electrostatic accelerator. Perfecting of the experimental facility enabled significant improvements to be made in the background conditions for the measurements and more reliable results to be obtained.

The method of experimental determination of the resonance self-shielding factor for capture cross-section f_c consists of using the capture cross-section $T_c(\tau)$ to measure the partial transmission and the total cross-section of $T_t(\tau)$ to measure the transmission. The cross-sections have the form

$$T_c(\tau) = \frac{N_c(\tau)}{N_c(0)} = \frac{\int_{\Delta E} \varphi(E) \sigma_c(E) \exp[-\tau \sigma_t(E)] dE}{\int_{\Delta E} \varphi(E) \sigma_c(E) dE};$$

where $N_c(\tau)$ and $N_n(\tau)$ are the number of readings by the capture event detector and the neutron detector for filter thickness τ ; $N_c(0)$ and $N_n(0)$ are the corresponding numbers of readings during exposure to an open neutron beam; $\varphi(E)$ is the form of the source neutron spectrum; $\epsilon(E)$ is the energy dependence on the efficiency of the neutron detector; and ΔE is the width of the spectrometer resolution function.

The value of the coefficient f_c can be derived from the values of $T_c(\tau)$ and $T_t(\tau)$, using the correlation:

$$f_c = \int_0^{\infty} T_c(\tau) d\tau / \int_0^{\infty} T_t(\tau) d\tau. \quad (1)$$

The transmission measurements were carried out on a neutron spectrometer by the time-of-flight method on the EG-1 FEHI accelerator (see figure). The main spectrometer parameters are as follows: duration of neutron burst - 4 ns, pulse period - 1.7 μ s; mean current - 2 μ A; flight path to capture event detector - 0.72 m, and to neutron detector - 0.51 m.

Transmission through the total cross-section $T_t(\tau)$ was measured by a detector with a thin (1.0 mm) ^6Li -glass, and the partial transmission $T_c(\tau)$ was measured by the self-indication method. Neutron capture events in the indicator sample with a thickness of 6.46×10^{-3} atom/b (^{235}U content $\leq 3.5 \times 10^{-3}\%$) were recorded by a 17 L-capacity scintillation detector. The filter samples of depleted metallic ^{238}U , in thicknesses of 2.37×10^{-2} , 4.74×10^{-2} and 9.43×10^{-2} atom/b, were placed at a distance of 26 cm from the accelerator target. The filter thicknesses chosen made it possible to measure transmissions of approximately 0.7, 0.5 and 0.3 respectively.

The neutron source was the $^7\text{Li}(p,n)^7\text{Be}$ reaction, and a thick lithium metal target was used. To reduce the neutron background of the location, the target was surrounded by a 4π -shield, the principal component of which was $\varnothing 26 \times 40$ cm cylinder, filled with a mixture of ^6LiH and paraffin. The neutron beam was formed by a section collimator consisting of ^6LiH rings with paraffin, borated polyethylene and lead. A $\varnothing 30 \times 15$ cm lead disk placed in front of the detector system was used to shield the capture event detector from gamma radiation arising in the accelerator target and the neutron shield, as well as natural radioactivity from the filter samples.

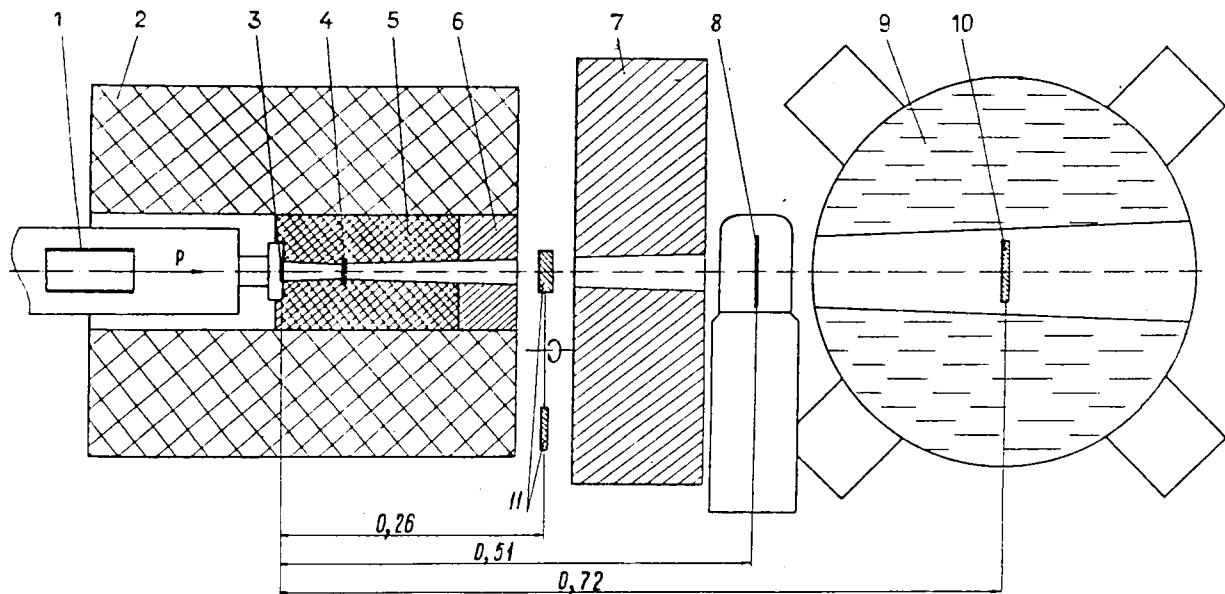
During the experiment particular attention was given to investigation of the background, which for the event capture detector can be divided into three components: constant, variable and instantaneous.

The constant background is governed by cosmic and natural radiations, and also the background of the measuring location coming from the neutron beam and operation of the accelerator. The shielding used in the experiment provided conditions in which the first two components of the constant background were at the same level as the background caused by the neutrons and the accelerator. In spite of a significant reduction in the constant background, it remained a determining factor and the ratio of effect to the constant background in the capture recording channel was 0.2, 0.9 and 1.9 at neutron energies of 10, 30 and 100 keV respectively. However, the value of this background component was determined with a sufficiently high degree of accuracy in each operational exposure, thanks to the use in the experiment of a 7 mm ^{23}Na filter permanently in position on the neutron beam ($E_0 = 2.85$ keV).

The variable background is associated with neutron capture in the shielding, the target structures and the collimator walls. The value of this component is insignificant (approximately 5% of the total effect) and is determined in experiments without an indicator sample.

The instantaneous background component is caused by recording by the detector of neutrons scattered in the indicator sample. The background represented 9, 3 and 1% of the net effect at energies of 10, 30 and 100 keV respectively and was determined in experiments with a graphite equivalent scatterer.

Investigation of the neutron detector background with ^6Li glass showed that it was constant in relation to the time of flight, and the background value was determined from the saturated resonance field of the ^{23}Na filter at an energy of 2.85 keV and the field between the γ peak and the beginning of the spectrum measured by time of flight. The ratio of the effect to the



Figure

Experimental layout: 1 - induction time marking sensor; 2 - neutron shield of ${}^6\text{LiH}$ with paraffin; 3 - neutron source (lithium metal target); 4 - ${}^{23}\text{Na}$ filter; 5 - collimating insert of ${}^6\text{LiH}$ with paraffin; 6 - lead insert; 7 - lead shielding; 8 - neutron detector with ${}^6\text{Li}$ glass (NE-912); 9 - liquid scintillation detector for capture events; 10 - ${}^{238}\text{U}$ indicator sample; 11 - ${}^{238}\text{U}$ filter samples

Table 1. Experimental f_c values for ${}^{238}\text{U}$

E_n , keV	f_c	Total error	E_n , keV	f_c	Total error
10-14	0,733	0,073	50-60	0,942	0,024
14-18	0,831	0,061	60-70	0,950	0,023
18-22	0,879	0,048	70-80	0,970	0,024
22-26	0,893	0,040	80-90	0,961	0,023
26-30	0,901	0,034	90-100	0,982	0,023
30-40	0,924	0,028	100-120	0,986	0,021
40-50	0,926	0,025	120-140	0,975	0,032

Table 2. Comparison of group values of f_c with BNAB evaluation data [4]

Group	ΔE_n , keV	f_c		Ratio
		Present study	BNAB	
11	10,0-21,5	$0,818 \pm 0,057$	0,830	1,015
10	21,5-46,5	$0,908 \pm 0,031$	0,910	1,002
9	46,5-100	$0,947 \pm 0,019$	0,938	1,012
8	100-200	$(0,982 \pm 0,023)$	0,986	1,004

background in the neutron channel was 1:1, 4:1, and 14:1 at neutron energies of 10, 30 and 100 keV respectively.

An important condition for transmission measurement is the constancy in time of the spectrum and the neutron source intensity, and hence the measurements with various filters were reflected in short series (approximately 2 min). The filter samples were changed automatically using a set of a specific current integral on the accelerator target with simultaneous switching of the time analyser memory group. There were two exposures with an open beam in the full measurement cycle. Comparison of the exposures showed that the systematic error in transmission measurement, relating mainly to the inconstancy of the intensity and spectrum of the neutron source, did not exceed 0.3%. The correction for the "dead time" of the recording apparatus was not more than 0.8%. Control measurements of carbon transmission (with filter thickness 8.6×10^{-2} atom/b), carried out simultaneously with uranium filters, showed that the measurement results for the total ^{12}C cross-section agreed with the ENDF/B-V assessment to within 2%, and the difference in transmissions obtained in the neutron and capture channels did not exceed 1%.

As a result of the measurements and processing carried out, energy dependences of the transmission values $T_c(\tau)$ and $T_t(\tau)$ were obtained from which the factors of capture cross-section resonance self-shielding were determined in accordance with expression (1). Data on the f_c factor in relation to the neutron energy are shown in Table 1, together with the total error comprising the statistical measurement error, the uncertainty of subtraction of background in time-of-flight spectra, the error associated with the procedure for deriving the f_c factor through expression (1), and the error caused by instability.

In order to compare the results obtained with the group values of the BNAB system of constants [4], the experimental data were averaged over the 1/E spectrum. This averaging is necessary since the spectrum of the neutron source used [the $^7\text{Li}(p,n)^7\text{Be}$ reaction] deviates strongly from the Fermi spectrum. The mean group values of the f_c factor and the total error are shown in Table 2. The good agreement (discrepancies of not more than 1.5%) of the results of these measurements with the BNAB data may be noted.

In conclusion, it should be noted that the use of expression (1) to obtain the f_c factor is a direct experimental method for evaluating the factors of capture cross-section resonance self-shielding. However, this method requires transmission measurements for large filter thicknesses, which is hindered by the decrease in the effect-to-background ratio, particularly in the capture event recording channel. For greater refinement of the f_c value, it would clearly be desirable to carry out a theoretical analysis of transmission measurements in the context of a model description of neutron transmissions through mean resonance parameters. Such an analysis should also make it possible to improve the accuracy of mean resonance parameter values for ^{238}U .

MEASUREMENT OF THE NEUTRON RADIATIVE CAPTURE CROSS-SECTIONS FOR
 ^{236}U AND ^{197}Au IN THE 3-420 keV ENERGY RANGE

L.E. Kazakov, V.N. Kononov, E.D. Poletaev, M.V. Bokhovko,
 A.A. Voevodskij and V.M. Timokhov

The neutron radiative capture cross-sections for ^{236}U and ^{197}Au in the 3-420 keV energy range were obtained. The measurements were carried out at the EG-1 FEH1 pulsed Van de Graaff accelerator using the time-of-flight technique. The saturated resonance was used for calibration and the $^6\text{Li}(n,\alpha)^3\text{H}$ and the $^{10}\text{B}(n,\alpha\gamma)^7\text{Li}$ cross-sections for flux shape.

The neutron radiative capture cross-section for ^{236}U is an important constant associated with the external fuel cycle, since neutron capture in this nucleus, together with other processes, determines the degree of accumulation of the radioactive nucleus ^{232}U , whose decay leads to the formation of powerful gamma emitters governing the radiation situation during fuel reprocessing. The requirements regarding exact knowledge of the capture cross-section for ^{236}U over a wide neutron energy range are quite stringent and amount to 7% [1]. However, the discrepancy between the few available experimental data [2-6] and evaluations considerably exceeds this value and on average attains 40%, while there are no data at all for the 50-160 keV range.

The purpose of the present study was to measure the capture cross-section for ^{236}U in the 3-420 keV energy range. Together with this, measurements were made of the neutron capture cross-section in ^{197}Au , which yielded the possibility of evaluating the reliability of the method used.

Measurement method and experimental set up. The experiment to measure radiative capture cross-sections was carried out with the fast and resonance neutron spectrometer at the pulsed Van de Graaff EG-1 at the Institute of Physics and Power Engineering (FEH1) (Table 1). The neutron capture events were recorded via the prompt gamma quanta by a 17-L liquid scintillation counter filled with a scintillator based on toluene with a 60% trimethylborate additive, which made it possible substantially to reduce the sensitivity of the detector to neutrons scattered in the sample. The neutron flux was measured by a detector with thin (1 mm) ^6Li -glass, located in front of the sample under investigation, and a detector consisting of a ^{10}B sheet and two NaI(Tl) crystals located behind the sample. For normalization of the cross-sections use was made of the saturated resonance method, making it possible to exclude direct measurements of the effectiveness of detection of the capture event and neutron flux [7-10]. In this case the capture cross-section can be written as follows:

$$\sigma_c = k \frac{N_c}{N_{\text{Li}}} \frac{1}{n} \frac{\sigma_\alpha}{T_m} \frac{S_{\text{Li}}}{S} \frac{\epsilon_\gamma^r}{\epsilon_\gamma}$$

where N_c and N_{Li} are the number of counts of the gamma detector and neutron monitor in measurements in the fast neutron region; n is the number of atoms per b in the sample under investigation; σ_α is the cross-section for the $^6\text{Li}(n,\alpha)^3\text{H}$ reaction; T_m is the capacity of the ^6Li -glass detector; S_{Li} is the correction for the final thickness of the ^6Li -glass; $S = F_S F_\gamma$ is the correction for the final thickness of the sample (F_S is the correction for multiple scattering and resonance blocking of neutrons in the sample, F_γ is the correction for gamma capture absorption in the fast neutron energy region);

and $\epsilon_Y^r/\epsilon_\gamma$ is the ratio of the degrees of effectiveness of the detector to capture events during measurement in the resonance and fast neutron energy ranges, as determined from an analysis of the measured amplitude spectra of the capture event detector. The normalizing coefficient k can be derived from experimentation in the saturated resonance region, using the relationship:

$$k = \frac{N_m^r}{N_c^r} P_c^r \frac{T_m^r F_\gamma^r}{\sigma_\alpha^r S_{Li}^r},$$

where the index r denotes the quantities in the energy resonance region, and the probability of neutron capture in the sample in the saturated resonance region is determined by the formula:

$$P_c^r = \left[1 - \exp(-n \sigma_t^r) \right] (\sigma_c^r / \sigma_t^r) F_{ms}^r.$$

Calculation of capture probability was effected by the Monte Carlo method, as a result of which values of 0.986 were derived for $^{236}\text{U}(E_0 = 5.45 \text{ eV})$ and 0.981 for $^{197}\text{Au}(E_0 = 4.906 \text{ eV})$.

Since the cross-section for the $^6\text{Li}(n,\alpha)^3\text{H}$ reaction can be used as a standard only up to an energy of about 100 keV, recourse was had at higher energies to a neutron detector with a ^{10}B sheet, and the shape of the capture cross-section measured with it was normalized on the basis of data obtained for the ^6Li -glass monitor. The capture cross-section in the energy range above 110 keV was determined by the formula:

$$\sigma_c = k_B \frac{N_c}{N_R} \sigma_{\alpha\gamma} \frac{T S_B}{S},$$

where k_B is the normalization coefficient; N_B is the number of detector counts with the ^{10}B sheet; $\sigma_{\alpha\gamma}$ is the cross-section for the $^{10}\text{B}(n,\alpha\gamma)^7\text{Li}$ reaction; T is the transmissivity of the sample under investigation; and S_B is the correction for the final thickness of the ^{10}B sheet.

The principal capture cross-section measurements, which were carried out with a flight base of 2.4 m (fast neutron and resonance region), yielded absolute values for the capture cross-sections in the 16-420 keV range. For extending the range downwards measurements were carried out with a flight base of 0.72 m, embracing the energy range 3-130 keV. The results of these measurements were normalized to the data derived with the flight base of 2.4 m.

Thus the experiment can be divided into three stages:

- Measurements in the 16-420 keV neutron energy range with a flight base of 2.4 m;
- Measurements in the resonance region with the same flight base;
- Measurements in the 2-130 keV energy region with a flight base of 0.72 m.

The geometry of the experiment for the 2.4 m flight base was kept unchanged in both the fast neutron and the resonance regions. For measurements in the 16-420 keV energy region, the detector system was installed in a room separated from the accelerator target by a concrete wall 2 m thick. Under these conditions measurements were carried out in the

Table 1. Parameters of the 5 MeV Van de Graaff accelerator

Parameter	Experiment		
	1	2	3
Proton energy, MeV	1,9	2,1	2,8
Neutron energy, keV	2-130	16-420	1-30 eV
Pulse duration, ns	4	5	0,5 μ s
Pulse period, μ s	1,7	2,2	140
Mean current, μ A	2	1,8	1,5
Flight base, m	0,51 (^6Li -monitor) 0,72 (LLSD)	2,2 (^6Li -monitor) 2,4 (LLSD) 2,7 (^{10}B -sheet)	2,2 (^6Li -monitor) 2,4 (LLSD)

Note: In experiments 1 and 2 the target was lithium metal, in experiment 3 it was lithium metal and a polyethylene moderator.

neutron energy region of a few electron volts. For obtaining neutrons of such energies the target was surrounded by a polyethylene moderator 1.6 cm thick.

Measurements in the 2-130 keV neutron energy range were effected on the short flight base. A short flight base makes stringent requirements on detector shielding and neutron beam collimation. The main component of the shielding was a cylinder 26 cm in diameter by 40 cm long, filled with a mixture of ^6LiH and paraffin, which surrounded the target. The neutron beam was shaped by a sectioned collimator of ^6LiH with paraffin and lead. The detectors were further shielded from the gamma radiation arising in the target and shielding by a massive lead disk 30 cm in diameter and 15 cm thick. The reliability of collimation and the adjustment of the system were experimentally tested using annular samples of ^{115}In placed in the capture event detector. Measurements showed that in the solid angles subtended by a sample 36 mm in diameter, 99% of the neutron beam was collimated. The use of this shielding substantially improved the background conditions of the experiment and made it possible to derive reliable data at low neutron energies, where output from the target is small.

Great attention was paid to study of the background. In order to be able to monitor the detector background at each exposure, the neutron beam was continuously covered by a metallic sodium filter 7 mm thick. The capture event detector background can be arbitrarily divided into three parts: constant, variable and instantaneous. The constant background, caused by cosmic radiation and natural radioactivity, also includes the measuring room background associated with the neutron beam and operation of the accelerator. Its value was determined at each exposure for two time-of-flight regions: between the gamma peak and the time of arrival of the fastest neutrons and in the "dark" resonance region in ^{23}Na at an energy of 2.85 keV. The variable background is associated with neutron capture in the shielding, the target structures and the collimator walls. The value of this component of the background is insignificant and can be derived with a high degree of accuracy by experimenting with an empty channel. The instantaneous component of the background results from the recording by the detector of neutrons scattered in the sample following their absorption in the scintillator and the detector envelope. This component was modelled using equivalent scatterers of graphite, ^{208}Pb , natural lead and bismuth oxide. Investigations showed that detector sensitivity to scattered neutrons was approximately 2×10^{-2} at a neutron energy of 5 keV, descending to 5×10^{-5} at an energy of 100 keV.

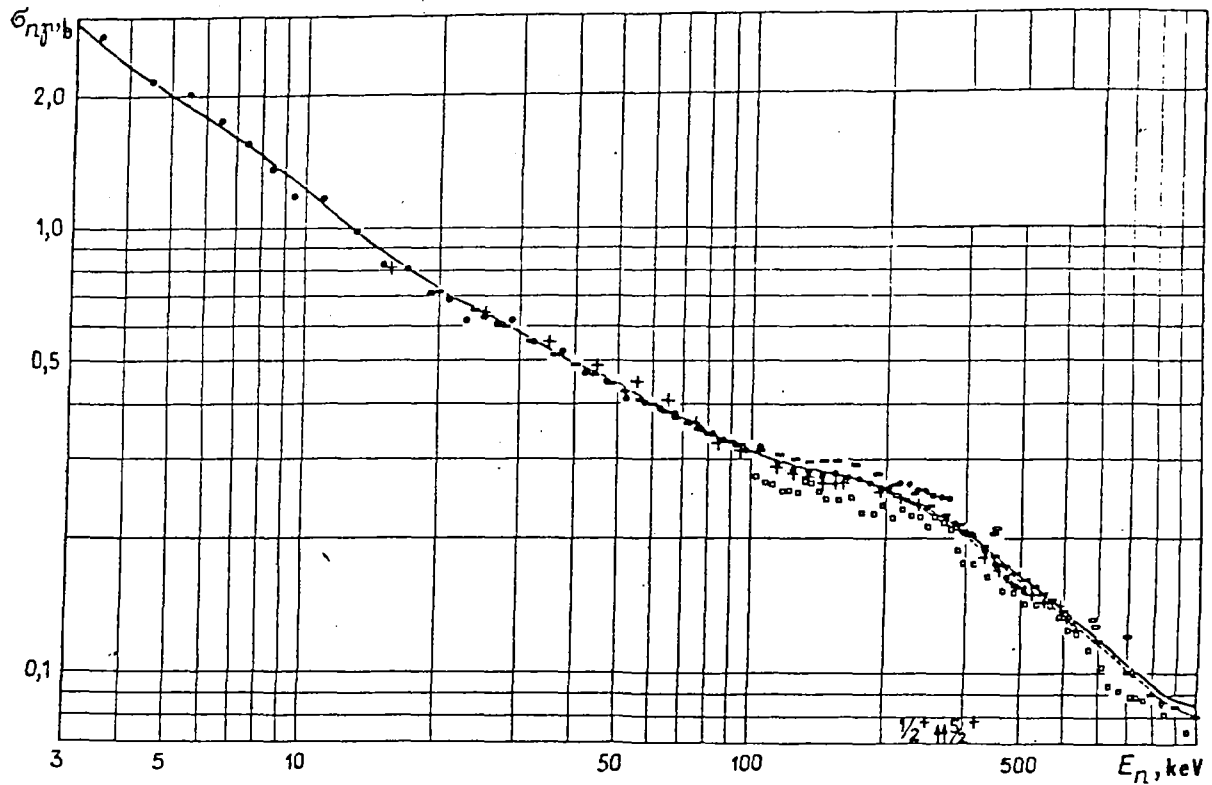


Fig. 1. Neutron radiative capture cross-section in ^{197}Au . Data: — — ENDL-78; - - - - ENDF/B-V; ■ — [11]; + — [12]; ○ — [13]; □ — [14]; ◇ — [15]; • — present study

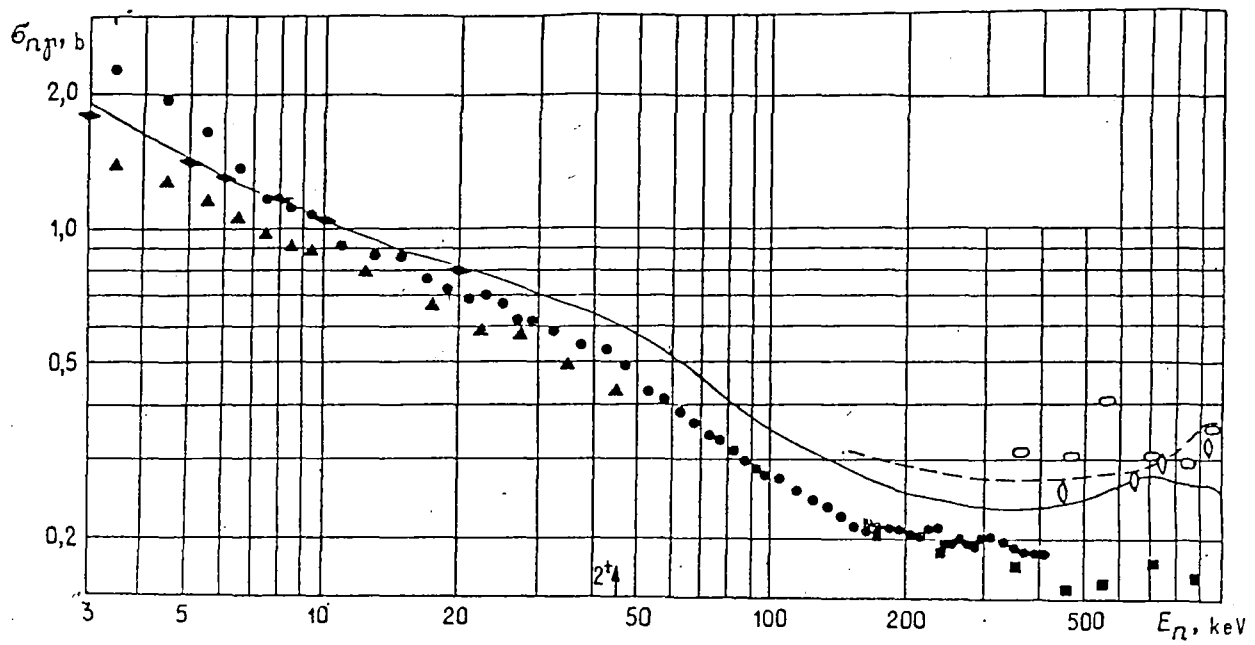


Fig. 2. Neutron radiative capture cross-section in ^{236}U . Data: — — JENDL-2; - - - - ENDF/B-V; ○ — [2]; ○ — [3]; ▲ — [4]; ■ — [5]; ◀ — [6]; • — present study

Table 2. Measurement error values

E, keV	Error, %											
	Statistical		Subtraction of background		Normalization		Relative shape of reference cross-sections		Introduction of corrections		Total	
	¹⁹⁷ Au	²³⁶ U	¹⁹⁷ Au	²³⁶ U	¹⁹⁷ Au	²³⁶ U	⁶ Li(n,p)	¹⁰ B(n,αγ)	¹⁹⁷ Au	²³⁶ U	¹⁹⁷ Au	²³⁶ U
5	3,4	4,3	4	8,1	—	—	0,5	—	—	—	6,4	10
10	1,5	1,9	1,3	3,2	—	—	1,0	—	—	—	4,2	5,5
30	1,0	1,2	0,5	0,5	—	—	2,0	—	—	—	4,3	4,6
100	0,9	1,0	0,5	0,5	2	2,1	2,0	—	3	3,3	4,3	4,5
200	1,2	1,9	0,5	0,5	—	—	—	1,6	—	—	4,2	4,7
300	1,3	1,7	0,5	0,5	—	—	—	2	—	—	4,4	4,7
400	1,0	1,1	0,5	0,5	—	—	—	2	—	—	4,3	4,6

The background of the ⁶Li glass neutron monitor, which is independent of the time of flight, was determined in the 2.85 keV region from the resonance of a ²³Na filter. The energy scale of the time analyser was calibrated using the narrow resonance of the ²³Na filter at an energy of 53.191 keV, recommended as a neutron energy standard when measuring by the time-of-flight method. The measurements were carried out in cycles, including experiments with sample, scatterer and empty channel. The samples used were 40 mm in diameter and consisted of ²³⁶U of thickness 0.00407 atom/b (²³⁵U content 0.047%) and of ¹⁹⁷Au of thickness 0.00458 atom/b. The samples were packed in light aluminium containers with wall thickness 0.007 mm.

The errors in the measurements of the capture cross-sections arise from several sources (Table 2).

The error associated with the introduction of corrections comprises: the uncertainty of corrections for the final thickness of sample, ⁶Li glass and ¹⁰B-sheet; the uncertainty of the correction for self-absorption of gamma photons in the sample; the error associated with possible divergence from unity of the ratio, ϵ_Y^E/ϵ_Y , of the respective degrees of effectiveness of the capture event detector in the resonance and in the fast energy regions; the error in taking account of the recording in the capture channel of gamma radiation from ²³⁶U fission below the barrier; and the uncertainty of the correction for the isotopic purity of the samples and the accuracy of determination of the number of nuclei.

Measurement results. The experimental results of measuring the fast neutron capture cross-sections for ¹⁹⁷Au and ²³⁶U are given in Table 3 and Fig. 1. It will be seen from the figure that the data from the present work are in good agreement with the results of studies [11, 12] in the energy region up to 100 keV. In the 100-200 keV range they lie below the data quoted in Ref. [11] by an average of 3-5%, but are in good agreement with the data from Ref. [12]. The results in Ref. [14] lie systematically lower than the present results by approximately 7-10%. Throughout the entire measured energy range our data are in good agreement with the evaluations of the ENDL-78 and ENDF/B-V libraries. In the energy region around 270 keV there is a distinct spread in the capture cross-section, caused by the opening of a competing neutron inelastic scattering channel with excitation of two levels (1/2⁺ for 268 keV and 5/2⁺ for 277 keV).

Our data on the capture cross-section for ²³⁶U are quite detailed. They clearly show the effect of competition from the opening neutron inelastic scattering channel with excitation of a collective 2⁺ level in ²³⁶U with

Table 3. Fast neutron capture cross-section, mb

E, keV	^{197}Au	^{236}U	E, keV	^{197}Au	^{236}U
3-4	2767±221	2275±303	7-8	1550±76	1166±86
4-5	2176±148	1929±220	8-9	1355±61	1101±70
5-6	2021±123	1647±165	9-10	1189±62	1086±63
6-7	1732±94	1376±117	10-12	1170±61	919±51
12-14	987±41	876±46	120-130	285±12	243±11
14-16	825±35	873±45	130-140	283±12	238±11
16-18	802±34	768±38	140-150	277±12	223±10
18-20	709±30	733±35	150-160	281±12	214±10
20-22	668±29	694±33	160-170	276±12	209±10
22-24	617±26	705±33	170-180	271±12	216±10
24-26	628±27	675±32	180-190	266±11	214±10
26-28	601±26	620±29	190-200	260±11	211±10
28-30	621±27	619±29	200-210	261±11	206±10
30-35	553±24	586±27	210-220	269±11	203±10
35-40	526±23	545±25	220-230	269±11	213±10
40-45	468±20	531±24	230-240	258±11	214±10
45-50	448±19	490±23	240-250	257±11	194±9
50-55	408±18	433±20	250-260	250±11	196±9
55-60	400±17	417±19	260-270	249±11	202±9
60-65	391±17	389±18	270-280	247±11	197±9
65-70	382±16	368±17	280-290	217±9	192±9
70-75	369±16	342±16	290-300	209±9	201±9
75-80	359±15	330±15	300-320	204±9	203±10
80-85	346±15	315±14	320-340	189±8	197±9
85-90	332±14	299±13	340-360	175±8	190±9
90-95	323±14	288±13	360-380	163±7	186±9
95-100	318±14	277±12	380-400	155±7	186±9
100-110	322±14	272±12	400-420	151±6	185±9
110-120	296±13	257±12			

an energy of around 45 keV (Fig. 2). In the 3-50 keV energy range the data from the present work are systematically lower (by approximately 15%) than those obtained in measurements in a lead cube [4], while in the energy region of a few electron volts the divergence attains 40%. In the energy range 160-400 keV our results are in good agreement with the data in Ref. [5]. The results of Refs [2, 3] are situated considerably higher (by approximately 40%).

The concordance of our results for the ^{197}Au capture cross-section with the latest experimental data and the most recent evaluations indicates the reliability of the measurement method applied. Hence, the results obtained, covering a wide neutron energy range and using a measurement method independent of those of other authors, can be regarded as satisfying the requirements regarding accurate knowledge of this constant.